IEEE Access
Multidisciplinary | Rapid Review | Open Access Journal

Received October 1, 2020, accepted October 11, 2020, date of publication October 22, 2020, date of current version November 11, 2020.

Digital Object Identifier 10.1109/ACCESS.2020.3033027

Recent Techniques and Trends for Retinal Blood Vessel Extraction and Tortuosity Evaluation: A Comprehensive Review

ALICE KRESTANOVA, JAN KUBICEK, AND MAREK PENHAKER, (Member, IEEE)
Department of Cybernetics and Biomedical Engineering, VSB - Technical University of Ostrava, 70800 Ostrava, Czech Republic

Corresponding author: Alice Krestanova (alice.krestanova@vsb.cz)

This work was supported in part by the Project Biomedical Engineering Systems XVI, under Grant SP2020/55, and in part by the research project The Czech Science Foundation (TACR) 440 ETA under Grant TL01000302 (Medical Devices Development as an Effective Investment for Public and Private).

ABSTRACT Retinal blood vessel segmentation plays an important part in the early diagnosis and treatment of eye disease. It is a tool for ophthalmologists. Many diseases can be identified by examining manifestations and images of blood vessels, including diabetic retinopathy, retinopathy of prematurity, age-related macular degeneration, retinopathy due to hypertension, glaucoma and others. Early detection allows physicians to provide patients with effective treatment, while in the opposite case, the late detection of retinal disease can ultimately lead to blindness. One of the indices when examining the retina is an evaluation of blood vessels based on tortuosity, i.e. the degree of curvature of blood vessels. This article presents a comprehensive overview of all segmentation techniques for retinal blood vessel extraction from images taken with a fundus camera in adults and older children or with a RetCam fundus camera in new-borns and younger children over the last 10 years. An integral part of this review is a comprehensive overview with information on all available public and private databases with retinal images. The review includes an evaluation of segmentation techniques based on objectivization parameters, including information on all objectivization parameters used in this article. As already mentioned, the degree of curvature of retinal blood vessels is used to classify severity of blood vessels tortuosity. There is no uniform metric for determining tortuosity, but this review presents a comprehensive overview of all metrics and calculations used to determine the degree of tortuosity of retinal blood vessels.

INDEX TERMS Review, retinal blood vessels, fundus camera, RetCam, retinopathy of prematurity, diabetic retinopathy.

I. INTRODUCTION

Retinal blood vessel segmentation is an important area in the field of ophthalmology [1]–[3]. A patient's retinal vasculature can be analysed by extracting blood vessels from retinal images. Prompt analysis allows physicians to make early diagnoses, evaluate disease, suggest appropriate treatment, and monitor disease progression [4]–[7]. Monitored diseases include diabetic retinopathy [5], [8], [9] and retinopathy of prematurity (ROP) [10], [11], while atherosclerotic retinopathy [12], haemorrhages [12], [13], age-related macular degeneration (AMD) [14], glaucoma [15]–[17] and hypertension [15], [17] are also diagnosed in databases. Table 4 clearly lists the databases used with established diagnoses.

The tortuosity or curvature of retinal blood vessels can be examined. It is one of the indicators of manifested eye disease. Blood vessel (vascular) tortuosity is associated with diabetic retinopathy, which affects people with diabetes mellitus or retinopathy of prematurity, a disease that affects premature infants [5], [10], [11]. This disease occurs due to the abnormal development of blood vessels. Ophthalmologists can determine the degree of these diseases or diagnose plus forms based on the degree of tortuosity. Left untreated, the disease can lead to blindness [18]–[20].

Tortuosity can also be a secondary symptom in, for example, people with high blood pressure, atherosclerosis and other diseases. Nevertheless, it is a common manifestation of

The associate editor coordinating the review of this manuscript and approving it for publication was Chulhong Kim.

age and small aberrations in blood vessel curvature occur in both humans and animals [21]. There is no gold standard for measuring the tortuosity of blood vessels that could be understood as the index for determining the degree of blood vessel curvature. To date, physicians evaluate tortuosity visually by comparing multiple images taken over time or manually using a contour gauge [11], [20].

Given the significance and clinical importance of retinal blood vessel tortuosity and the potential of image segmentation methods, modern trends are focusing on the development of fully automated methods that allow the selection of blood vessels from the retinal background with the aim of creating a mathematical model that can identify the vascular system from other retinal components. This model has the potential to calculate the geometric parameters of the vascular system corresponding to the curvature of each element thereof. Such parameters have the potential to quantify the degree of tortuosity as a parameter that permits the evaluation of the degree of pathological changes to the vascular system on the basis of abnormal curvature. Such systems are of extreme importance for clinical practice in the sense of automating manual clinical procedures, which are thus refined and objectivised. Programs for the semi-automatic measurement of tortuosity using software such as ROPtool are being tested at some workplaces [22].

This publication presents a comprehensive review of recent scientific literature focusing on two essential aspects in the development of systems for the clinical evaluation of tortuosity. The main topic of the publication is an overview and analysis of recent methods for the segmentation of retinal images in the context of identifying the vascular system and subsequent analysis of mathematical models for the calculation of tortuosity.

The publication is structured as follows. Section II deals with the structure of the review for blood vessels segmentation and calculation of tortuosity. Period from 2010 to 2020, keywords (blood vessels segmentation, fundus camera etc.) were important for selection articles. Databases Scopus, Web of Science, Google Scholar etc. were searched. More information about structure of review is in this section.

Section III contains information about the available retinal databases used in articles. In this section were describe open access databases and private databases with retinal images taken by fundus camera. In the tables were shown name of database, type of modality, disease, university/hospital. Quantity of used databases in selected articles were graphically summarized. Diagnosed diseases from databases were graphically summarized. The most used databases were open databases DRIVE and STARE.

Section IV describes the segmentation algorithms for retinal blood vessel extraction divided into groups according to the common principle of the segmentation method. This chapter is further divided into subsections in which each group is clearly described. Overview tables are created in each subsection. These tables include authors with references, year of publication, used dataset, specified used method and values of evaluation parameters (accuracy, specificity, sensitivity). The methods with the highest value of accuracy (Acc) were highlighted in green for database DRIVE and STARE in every subsection.

Subsection A represents methods based on region-based deformable models. Subsection B represents methods based on multi-scale segmentation. Subsection C represents segmentation methods based on morphological operations. Subsection D includes methods based on adaptive thresholding. Subsection E describes methods with tracking approaches. Subsection F contains methods kernel-based algorithms for segmentation retinal blood vessels. Subsection G is divided into part supervised methods and methods based on CNN. Subsection H contains unsupervised machine learning. Subsection 22 is overview subsection with evaluating of described methods based on used evaluation parameter.

Section V describes the objectivization parameters used to evaluate the effectivity of the algorithm. Parameters such as: accuracy (Acc), specificity (Sp), sensitivity (Se), ROC curve, AUC, MSE, MCC, DSC, PPV, F1 score, AMTR and FMTR were described here based on our knowledge.

Section VI contains information about the mathematical calculations used to describe and calculate the tortuosity or degree of blood vessel curvature in retinal images. An overview table with authors, year, dataset, methods is also included.

II. STRUCTURE OF THE REVIEW

The Section II contains information about structure of the review. The articles were used in time period from 2010 to 2020. For review of segmentation blood vessels were selected articles based on keywords (retinal images, image segmentation, blood vessels, vasculature, fundus camera etc.) in the first part of review. Keywords (tortuosity, curvature, blood vessels, metrics, index etc.) were used for selection of articles in the second part of review calculation of blood vessel tortuosity. Articles were searched in databases Scopus, Web of Science, Google Scholar etc. More information is below in the Section II.

This review presents an overview of segmentation methods for retinal blood vessel extraction and metrics for the calculation of blood vessel tortuosity.

Articles and studies selected for this review date from 2010 to the 2020 in order to ensure the overview of segmentation methods used for blood vessel segmentation is as up to date as possible. When deciding whether to use articles, keywords such as retinal images, image segmentation, blood vessels, vasculature, fundus camera, Retcam, diabetic retinopathy, retinopathy of prematurity, supervised and unsupervised machine learning, morphological operations, fuzzy, multi- scale, were decisive.

The review of segmentation methods for blood vessel extraction therefore focused solely on retinal images of adults and children. Articles were selected from websites such as: Scopus, Web of Science, Google Scholar, PubMed, Semantic Scholar, IEEE Xplore.

TABLE 1. Overview of articles selected for the review of the blood vessel segmentation methods in retinal images.

Type of article	Number of journals with IF factor
Q1	35
Q2	21
Q3	5
Q4	2
Conference, symposium, workshop	52

TABLE 2. Overview of articles selected for the review of the metrics and calculation of blood vessel tortuosity.

Type of article	Number of journals with IF factor
Q1	3
Q2	3
Q3	1
Q4	1
Conference, symposium, workshop	10

The text contains 115 articles from Q1 to Q4 journals, but also conference articles, because based on set criteria, this area is not sufficiently comprehensive and examined in Q1 journals only. The composition of articles for this review is shown in Table 1 below. Segmentation methods for blood vessel extraction were divided into subsections based on the principle of segmentation, i.e. region-based deformable models, multi-scale segmentation, morphological operations, adaptive thresholding, tracking approaches, kernel-based algorithms, supervised and unsupervised machine learning.

This review also provides an overview of the available public and private databases of retinal images used, including the number of images in these databases and the camera with which they were taken. It includes the name of the organisations that participated in the creation of the database or dataset. The review includes a chapter on the objectivization parameters used in articles and studies to determine the quality of the segmentation algorithm.

The following part of the review provides an overview of metrics for the calculation of retinal blood vessel tortuosity. Once again, this review includes articles from 2010 to the present, in order to provide an up-to-date overview of this area. When deciding whether to use articles, keywords such as retinal images, tortuosity, curvature, blood vessels, metrics, index, classification, calculation, evaluation, diabetic retinopathy, retinopathy of prematurity, were decisive.

The review of different metrics of tortuosity or blood vessel curvature focused on retinal images only, where tortuosity was mainly examined for diabetic retinopathy or retinopathy of prematurity (see Table 19). Articles were selected from websites such as: Scopus, Web of Science, Google Scholar, PubMed, Semantic Scholar, IEEE Xplore. A total of 18 articles that met the criteria were selected. Table 2 shows the number of articles of the given type used by quartile.

III. DATABASES OF RETINAL IMAGES

The Section III deals with open access (public) and private databases of retinal images. The mostly used databases are DRIVE and STARE. This section includes overview tables with name of database, modality, university/hospital, diseases. Databases contains pathological and physiologically healthy images. The disease is classified for retinal images for each database. The section includes graph with plotted diseases from databases. The mostly classified diseases in database is diabetic retinopathy. Databases have variable resolution, various diseases, captured by different fundus cameras mostly in adults, across databases. More information is below in the Section III.

Segmentation algorithms were applied to datasets from two basic fundus camera modalities. This relates to a widely used colour fundus camera for capturing retinal images in adults and older children and a fundus camera called a RetCam3, which is used to capture retinal images in premature infants up to approx. 1 year of age [11] or RetCam 130 for younger children [18].

A substantial part of the research carried out on retinal blood vessel segmentation is applied to medical data from open access (public) databases. These are most often DRIVE [23] and STARE [12], which offer native images, but also already segmented images to enable an evaluation of the effectivity of the proposed algorithm. The advantage of these databases is that they have a defined gold standard, which is important for evaluating the effectivity of the algorithm. These databases include, among other things, images of the retina with diabetic retinopathy, haemorrhages, age-related macular degeneration (AMD), glaucoma, neoplasms and hypertension.

There is no open access database for examining the retinal blood vessels of premature infants, who usually suffer from retinopathy of prematurity (see Table 4). For this reason, it is difficult to classify or evaluate the quality of proposed segmentation algorithms in this area.

Table 3 provides an overview of open access (public) and private databases, including the type of modality by which the data was scanned. The table also contains the names of the institutions that are the authors and original researchers of the databases. Retinal images of patients were taken with fundus cameras by Canon, TopCon, Zeiss, Optos, EasyScan SLO. In new-borns, the retina was scanned using a RetCam3 or RetCam130 fundus camera.

Table 4 provides an overview with more detailed information about individual databases in terms of dataset size, image resolution and classification of the types of disease in the images.

A. OPEN ACCESS (PUBLIC) DATABASES

The open access DRIVE database and STARE database are among the most widely used datasets for working with retinal images (see Fig. 2). These datasets are popular due to the good resolution of retinal fundus images. DRIVE has a

TABLE 3. Overview of available open access and private databases with retinal images.

Database	Modality	University/Hospital
DRIVE [23]	Canon CR5 non-mydriatic 3CCD	A diabetic retinopathy screening programme in the Netherlands
STARE [12]	TopCon TRV-50	University of California and Veterans Administration Medical Center in San Diego, USA
ARIA [14,24]	Zeiss FF450+ fundus camera	St. Paul's Eye Unit, Royal Liverpool University Hospital Trust and Department of Ophthalmology, Clinical Sciences, University of Liverpool, Liverpool, UK
CHASEDB [25]	Top Noc TRV-50	Kingston University London
HRF [16]	Canon CR-1 fundus camera	Pattern Recognition Lab (CS5), the Department of Ophthalmology, Friedrich-Alexander University Erlangen-Nuremberg (Germany), and the Brno University of Technology, Faculty of Electrical Engineering and Communication, Department of Biomedical Engineering, Brno (Czech Republic)
IMAGERET [26, 27]	Fundus camera (not precisely specified)	Lappeenranta University of Technology, Finland
MESSIDOR [28]	Topcon TRC NW6 non-mydriatic	Messidor program partners and LaTIM laboratory Brest University Hospital, France
VICAVR [29]	TopCon non-mydriatic camera NW-100	Varpa Research Group, University of Coruna, Spain
ROC [13]	TopconNW100 TopCon NW 200 Canon CR5-45NM	Department of Electrical and Computer Engineering, University of Iowa, Iowa, USA
REVIEW [30] (HRIS)	Cannon 60 UV film camera	Department of Computing and Informatics at the University of Lincoln, UK
REVIEW [30] (VDIS)	Zeiss fundus camera and JVC 3CCD	Department of Computing and Informatics at the University of Lincoln, Lincoln, UK
REVIEW [30] (CLRIS)	Zeiss FF 450 fundus camera and JVC 3CCD	Department of Computing and Informatics at the University of Lincoln, Lincoln, UK
REVIEW [30]	Canon 60 UV fundus camera	Department of Computing and Informatics at the University of Lincoln, Lincoln, UK
IOSTAR [31]	EasyScan SLO camera	Biomedical Engineering at Eindhoven University of Technology (TU/e, Eindhoven, the Netherlands) Northeastern University (NEU, Shenyang, China Shengjing Hospital, Shenyang, the Maastricht Study, Netherlands Eye Care, Shenyang
DRIONS DB [15]	Fundus camera (not precisely specified)	Ophthalmology Service at Miguel Servet Hospital, Saragossa, Spain
DR HAGIS [17]	Topcon TRC – NW6s Topcon TRC – NW8 Canon CR Dgi fundus camera	Faculty of Biology, Medicine and Health, University Manchester, UK
VAMPIRE [32]	Canon CR-Dgi nonmydriatic OPTOS p200	University of Dundee, UK University of Palermo, Italy University of Verona, Italy University of Edinburgh, UK Clinical Research Imaging Centre, UK Ninewells Hospital, UK Princess Alexandra Eye Pavilion, UK and others
RetCam3 database [11]	RetCam3 camera	Centre for Children with Eye Defects, Department of Ophthalmology, University Hospital Ostrava Biomedical Engineering, Faculty of Electrical Engineering and Computer Science, Technical University of Ostrava
TROPIC database [33]	RetCam130 camera	Alberta Children's Hospital, Calgary, Canada
RET-TORT [34]	Topcon TR50 fundus camera	University of Padova, Italy

resolution of 768×584 pixels and STARE has a resolution of 650×700 pixels, with the possibility of using images already segmented by experts as the gold standard.

Table 4 below lists databases with more detailed information on the properties of the images, i.e. their resolution, the size of datasets, and the composition of images with information about the indicated disease. Datasets contain images that include, for example, physiological images of healthy patients, diagnosed diseases such as diabetic retinopathy, atherosclerosis, hypertension, embolism, and more (see Table 4). More detailed information on classified diseases and in how many datasets they are diagnosed is shown below in the graphic overview Fig. 1.

The graph below (see Fig. 1) clearly shows the number of databases in which the classified diseases were diagnosed. Diabetic retinopathy was the most frequently diagnosed disease in 12 databases. Physiological images were in 6 databases and the composition of data was not further specified in 5 databases.

The graph below shows the use of open access databases in the articles covered in this review. The most frequently proposed segmentation procedures were for images from DRIVE in 105 articles and STARE in 68 articles, which are open access and have gold standards, thanks to which the proposed algorithm can be objectively evaluated. The third most frequently used database was CHASE or CHASEDB in 16 articles, followed by HRF, REVIEW, ARIA, the RetCam3 database, TROPIC, RET-TORT, VAMPIRE (see Fig. 2).

DRIVE (Digital Retinal Image for Vessel Extraction) contains 40 images that were randomly selected from images taken from a total of 400 people aged from 25 to 90 during screening. The dataset contains 33 physiological images of the retina without symptoms of diabetic retinopathy and

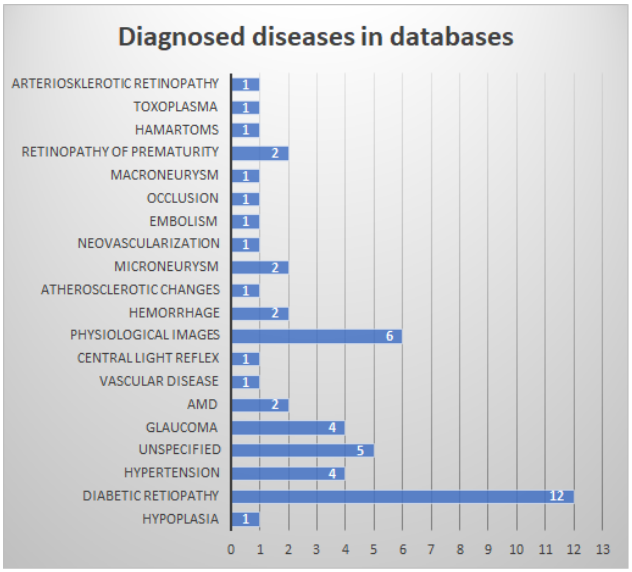

FIGURE 1. Graphic overview of diagnosed diseases in datasets.

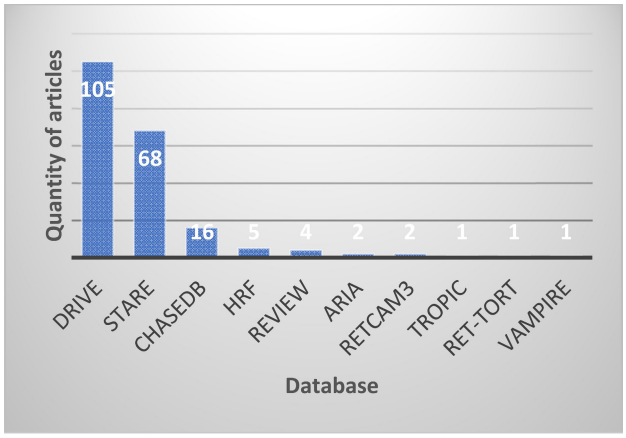

FIGURE 2. Graph of databases used for the application of segmentation algorithms for blood vessel extraction.

7 images with symptoms of mild, early retinopathy. The data is saved in JPEG format. The dataset was divided into a training and test set, each containing 20 images. The images in the test set were segmented by two experts and can be considered as the gold standard [23].

STARE (Structured analyses of the retina) contains 400 images of the retina, with 40 images containing manually segmented blood vessels. The disease is specified for each image in consultation with an ophthalmologist. The output of segmentation are binary images. The data was compressed into PPM format [12].

ARIA (Automatic Retinal Image Analysis) contains 143 images that are divided into three groups: a healthy control group, a group with age-related macular degradation and group with diabetes. A reference standard was created for each image in the database by two experts, who examined

TABLE 4. Overview table with more detailed information about databases.

Database	Resolution [pixel]	Size of dataset	Disease
DRIVE [23]	768x584	40	33 control group 7 mild, early diabetic retinopathy
STARE [12]	650x700	400	Diabetic retinopathy, arteriosclerotic retinopathy, occlusion, hypertension, embolism, choroidal neovascularisation, macroaneurysm,
ARIA [14,24]	768x576	143	23 AMD 59 diabetes 61 control group
CHASEDB [25]	1280x960	28	Not specified
HRF [16]	3304x2336	45	15 physiological images 15 diabetic retinopathy 15 glaucoma
ImageRet [26, 27] (DIARETDB1)	1500x1152	89	5 diabetic retinopathy 84 mild, proliferative diabetic retinopathy
ImageRet [26, 27] (DIARETDB0)	1500x1152	130	20 control group 110 diabetic retinopathy
MESSIDOR [28]	1440x960 2240x1488 2304x1536	1200	diabetic retinopathy number of microaneurysms
VICAVR [29]	768x584	58	Not specified
ROC [13]	768x576 1058x1061 1389x1383	100	diabetic retinopathy, microaneurysms, haemorrhages
REVIEW [30]	1360x1024 to 3584x2438	16	8 high resolution 4 vascular disease 2 central light reflex 2 kick point
REVIEW (HRIS) [30]	3584×2438	4	diabetic retinopathy
REVIEW (VDIS) [30]	1360x1024	8	diabetic retinopathy
REVIEW (CLRIS) [30]	2160x1440	2	atherosclerotic changes
REVIEW (KPIS) [30]	3300x2600	2	Not specified
IOSTAR [31]	1024x1024	30	Not specified
DRIONS DB [15]	600x400	110	Chronic simple glaucoma, hypertension
DR HAGIS [17]	4752x3168 3456x2304 3126x2136 2896x1944 2816x1880		10 glaucoma 10 hypertension 10 diabetic retinopathy 10 age-related macular degeneration
VAMPIRE [32]	400x400 3000x3000	8	Not specified
RetCam3 database [11]	640x480	2793	retinopathy of prematurity physiological images haemorrhages Toxoplasma Hypoplasia hamartoma
TROPIC database [33]	640x480	130	30 ROP 1 30 ROP 2 20 ROP 3 30 physiological images
RET-TORT [34]	1300x1100	60	Retinopathy in hypertensive and healthy patients

the blood vessels, optic disc and macula. Data was scanned in TIFF and converted into JPG format [14], [24].

CHASEDB consists of two sets of manually segmented monochrome ground truth images. These images were segmented by two experts. It contains 28 images with a resolution of 1280 × 960 pixels [25].

There is a total of 45 images in the open access ***HRF*** (High Resolution Fund) database, sometimes called the Erlangen database in the article [35]. Images are colour, in JPEG format with low compression. A binary mask is created for each image for further analysis. The binarized image of blood vessels represents the gold standard. Masks determining the field of view (FOV) can be used for certain parts of datasets. The gold standard for images is set by a group of retinal image analysis experts and ophthalmologists at an optical clinic [16].

IMAGERET is an open access database, which consists of two parts - DIARETDB0 and DIARETDB1. Images are saved in PNG format. The dataset also contains reference standards and an evaluation script in MATLAB. DIARETDB0 contains 130 images, with 20 images from the control group and 110 images with signs of diabetic retinopathy. DIARETDB1 contains 5 images with diabetic retinopathy and 84 images with mild manifestations of proliferative diabetic retinopathy [26], [27].

MESSIDOR (Methods to Evaluate Segmentation and Indexing Techniques in the field of Retinal Ophthalmology within the Scope of Diabetic Retinopathy) is an open access database that was primarily designed to compare and evaluate different segmentation algorithms for the detection of lesions. Images are saved in TIFF format. Medical diagnoses are available for each image with the defined degree of diabetic retinopathy in an Excel file. Images were taken in patients aged 25 to 65 [28].

VICAVR contains 58 retinal images. It is used to calculate the artery/vein ratio. The database focuses on the optic disc, but also arteries/veins in different radii from the optic disc. These arteries/veins were identified by three experts [29].

ROC (Retinopathy Online Challenge) contains 3 different types of images with different resolutions, as they were captured using three different fundus cameras (see Table 3). Images were saved in JPEG format. The database can be divided into two parts: 50 training images and 50 test images [13].

REVIEW (Retinal Vessel Image Set for Estimation of Widths) consists of 4 high-resolution HRIS datasets, VDIS (vascular disease image set), CLRIS (central light reflex image set) and KPIS (kick point image set). Images have a higher resolution than images in the DRIVE database [30].

IOSTAR contains 30 images captured by a laser fundus camera. The images were edited by two different experts, the same ones as the DRIVE dataset [31].

110 retinal images from a total of 124 images captured by a fundus camera in ophthalmology at Miguel Servet Hospital in Saragossa (Spain) were selected for the ***DRIONS DB*** database. A total of 14 images were discarded because they contained moderate or severe cataracts. The average age of patients was 53. The database contains retinal images from 46.2% men and 53.8% women [15].

The ***DR HAGIS*** dataset was created as part of a screening programme for diabetic patients in the United Kingdom. The images were obtained at different screening centres, and for this reason have different resolutions. The images were captured using different types of fundus cameras. All were saved in JPEG format. The dataset also offers a gold standard for comparison [17].

VAMPIRE (Vascular Assessment and Measurement Platform for Images of the Retina) is a dataset of images from a fundus camera and software for semi-automatic detection of retinal blood vessels. It is the result of international cooperation by 4 groups in image processing and 5 clinical centres. More information is available here:

https://vampire.computing.dundee.ac.uk/news.html [32].

The RetCam3 DATASET is a private database that was created as a result of screening premature infants. The data was obtained by the Centre for Children with Eye Defects in Ostrava and processed for the purpose of segmentation by the Department of Biomedical Engineering of the Faculty of Electrical Engineering and Computer Science. The images were taken with a RetCam3 camera with a resolution of 640 × 480 pixels.

Data was anonymised. Screening took place for 40 boys and 40 girls. The images show observable structures such as the blood vessels, optic disc and pathological formations, such as lesions or haemorrhages. The images are significantly different from each other, they have different contrast and brightness properties. These are images of premature infants, so, among other things, there is a large number of choroidal vessels or artefacts caused by the movement of the child's eyes. The dataset clearly shows the gestational age of the child at the time of birth and their birth weight [11], [36], [37].

Gestational age at birth ranges from 24 to 41 weeks in this dataset. The highest percentage of 53% is a gestational age at birth of 33-41 weeks, 32% are children born at 29-32 weeks, and 15% in the dataset represents 12 children of a gestational age of 24-28 weeks at birth (see Fig. 3).

The birth weight of premature infants and term infants was also recorded in the dataset (see Fig. 4). The composition of birth weight is as follows: 59% are patients with a birth weight of more than 1500 g (number of patients: 47), 24% are 19 patients with a birth weight of 1000 to 1499 g and 17% with a birth weight of less than 1000 g (number of patients: 14) [38].

TROPIC (Telelemedicine for ROP in Calgary) is a private database of retinal images taken in 41 premature infants. The images were taken with a RetCam130 wide-angle camera with a resolution of 640 × 480 pixels. There is a total of 130 images in the database. Subsequently, 110 images were selected at random, in which the stage of retinopathy of prematurity was determined. 30 images were determined to have no diagnosis, 30 images had 1st degree ROP, 30 images had 2nd degree ROP and 20 images had determined 3rd degree

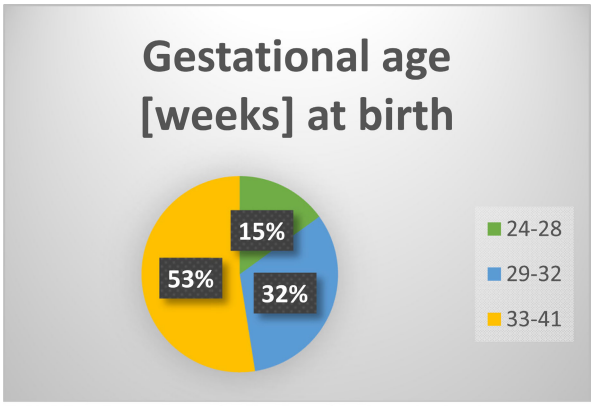

FIGURE 3. Percentage distribution of patients in the dataset according to gestational age.

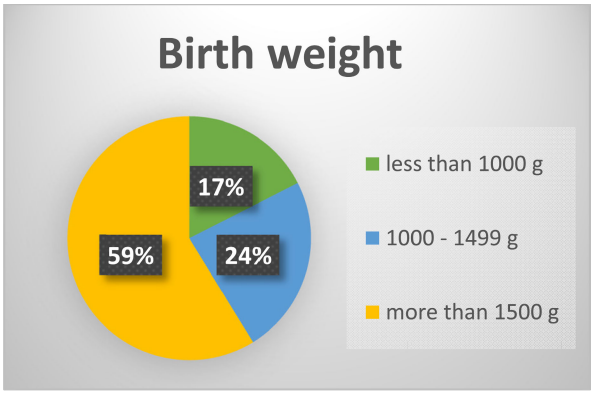

FIGURE 4. Percentage distribution of patients in the dataset according to birth weight.

ROP. Of these, 91 images were asymptomatic plus disease [33].

RET-TORT is an open access database. It contains 60 retinal images from healthy and hypertensive patients with information on estimated tortuosity. The dataset can be downloaded here:

http://bioimlab.dei.unipd.it/Retinal%20Vessel%20Tortuosity.htm [34].

IV. SEGMENTATION ALGORITHMS FOR BLOOD VESSELS EXTRACTION

In a general way, the image segmentation is a process of extracting objects that are in the user's foreground and suppressing unwanted objects in the background by using specific image intensity or geometric features. In this way, only the given parts are segmented. Retinal images are composed of observable objects as retinal blood vessels, optical disc and retinal pathologies, including retinal lesions which are standardly object of the retinal image segmentation. Retinal blood vessels are composed of retinal veins, arteries, possibly choroidal vessels which should be identified within the retinal image segmentation.

Segmentation of retinal blood vessels is a process for extraction and identification of retinal blood vessels. Images in databases have different resolution because images are taken by different fundus cameras. Therefore, segmentation algorithms utilize various approaches with different effectivity in particular retinal dataset as we report in this review. A challenging issue in the retinal image segmentation is building versatile segmentation algorithms which will have the same effectivity for various retinal images and will be sufficiently robust against image noise and artefacts, which can occur in retinal images.

The retinal blood vessel segmentation procedures are frequently completed with the image pre-processing methods. Blood vessel pre-processing is utilized before starting the segmentation procedure. Images are pre-processed, which is designed to optimise the brightness of blood vessels and eliminate image noise. The image pre-processing is generally aimed on improving the retinal image area and increase accuracy of segmentation methods. These procedures have the potential to optimise the effectivity and robustness of segmentation procedures. The first step in pre-processing is to convert the colour image to greyscale, the next steps are: suppression of image noise (image filtering), improving contrast and brightness transformation [11], [36], [39]–[41].

Images come from different modalities, so they have different resolutions, amount of noise and contrast. For this reason, it is necessary to approach image pre-processing in different ways.

The next part of this section is devoted exclusively to aspects of segmentation procedures. Manual segmentation, semi-automatic and automatic methods are used to extract blood vessels from retinal images.

Manual segmentation is time consuming and is not repeatable or reproducible. It requires certain experience and effort to properly set segmentation procedures. For semi-automatic and automatic methods, the cooperation of at least one expert ophthalmologist is necessary to evaluate the segmentation results. Automatic segmentation of retinal blood vessels is a step towards the development of a computer diagnostic system for eye disease [42]–[44].

A suitable indicator of the quality and effectivity of the segmentation algorithm is a comparison with the gold standard of open access databases.

In general, segmentation methods for extraction of retinal blood vessels can be divided into the following subcategories: subsection A contains methods based on region-based deformable models, subsection B includes multi-scale segmentation, subsection C contains methods based on morphological operations, subsection D contains method used adaptive thresholding, subsection E includes tracking approaches, subsection F kernel-based algorithms, subsection G contains supervised segmentation methods and subsection H contains unsupervised machine learning. The last subsection I is a summary chapter with evaluation of individual methods based on Acc parameter.

TABLE 5. Overview of the division of segmentation methods for retinal blood vessel extraction into groups.

Type of method	Number of publications	Reference
Region-based deformable models	9	7, 45-51, 155
Multi-scale segmentation	7	6, 41, 52-56
Morphological operations	9	9, 11, 18, 38, 57-61
Adaptive thresholding	6	5, 35, 44, 62- 64
Tracking approaches	11	1, 65-74
Kernel algorithms	11	19, 75-83, 156
Unsupervised machine learning	20	3, 20, 36, 39, 41, 83 -97
Supervised machine learning	46	2, 8, 98-141

In each subsection of this group of segmentation methods, the values of objectivization parameters with the best result are marked in green. Subsequently, the most effective method was chosen by a comparison of the identified parameters in the group. This method is coloured green with the appropriate dataset in which segmentation was successful. It is difficult to unequivocally define which method is most effective for the use of the segmentation algorithm to extract retinal blood vessels. There are certain limitations here, as the authors did not uniformly use a certain type of dataset with a certain number of samples and did not use the same objectivization parameters to determine the quality of algorithms or they were not objectively evaluated at all.

The most frequently used datasets are DRIVE and STARE (see Fig. 2) and the most frequently used parameters are Acc (accuracy), Sp (specificity) and Se (sensitivity) (see Table 5 - XIV). The best method for extracting blood vessels from images in the DRIVE and STARE database was determined in each group by green colour. A more detailed breakdown by type of segmentation method and number of publications used is given in Table 5 below.

A. REGION-BASED DEFORMABLE MODELS

Segmentation using deformable models is based on the deformation of an initialized curve or surface so that their energy is minimized. Within segmentation retinal blood vessels based on deformable model, the following methods are available Chan Vase, LBF (Local Binary Fitting) and active contours driven by local Gaussian distribution fitting energy. More information is below in this section.

Deformable models can be divided into parametric and geometric models. These are approaches that use the action of internal and external forces, on the basis of which the image is deformed with the segmentation of curves or surfaces in the image.

Region-based deformable models enable the separation of the foreground from the background of the image based on the assumption that each of these parts is statistically homogeneous. The main difference in the algorithms used is the type of statistics used to describe the regions. This is a suitable method for the segmentation of images where there is a problem with edge detection, such as noisy images or images with non-uniform brightness. Region-based deformable models also depend on the choice of initialisation location for segmentation. In contrast to edge detector-based image segmentation methods, region-based deformable model algorithms are more computationally intensive.

The authors use segmentation techniques such as active contours or snake contours. ***Active contours*** can be further divided into, for example, Chan Vase, LBF (Local Binary Fitting) and active contours driven by local Gaussian distribution fitting energy, which describes the local intensity of the image with different deviations and diameters [45], [49].

Another method classed as a deformable model is the ***level set*** method based on information on local clusters in regions that form a non-homogeneous image of the retina [47]. Chen *et al.* use a combination of a level set function with established selective binary and Gaussian filtering in combination with LBF to work with low contrast images [45].

The graph cut is the next method based on an energy-based object segmentation. The main idea of this method an optimization operation designed to minimize the energy generated from a given image data. The relationship between neighbourhood pixel elements in an image is defined by the energy [156].

Combination of graph cut and active contours is existed for better segmentation result. The graph cuts-based active contour method is used for blood vessel segmentation, as this method is effective for pre-processed images using a local phase filter [7].

Further development of this method consisted of the use of a local phase filter, again in combination with active contours, but with infinite perimeter active contours. By setting an infinite perimeter, the segmentation algorithm is more suitable for vessel detection than by using the conventional shortest length [46].

Zhang *et al.* modified the active contour method using correlational open active contours, i.e., each edge is segmented based on the active contour, which is initialised by the corresponding boundary of the Hessian response [46].

Wang *et al.* modified the region-based active contour method, which takes into account the intensity of the image and value of the vessel after local phase enhancement as two independent variables for the construction of multifunctional local Gaussian distribution fitting energy. This improves the segmentation procedure of active contours [49].

Xiao *et al.* describe the use of the level set function based on the Bayesian method, which takes into account the spatial information in the image. The boundaries of blood vessels are obtained, which are further used to minimise the energy function in the level set [50].

Dizdaroglu *et al.* approach the application of the level set method based on the selection of sampling seed points for blood vessel segmentation [51].

Table 6 presents a complete overview of segmentation methods in the field of methods based on region-based segmentation for retinal blood vessel extraction.

Based on the conditions specified in Section IV, the best method for retinal blood vessel extraction in this category appears to be the active contour method according to Zhao *et al.* [46].

Due to the consistency of the tables, the table below does not contain these parameters AU ROC in articles Zhao *et al.* [7], Zhao *et al.* [46], Zhang *et al.* [48], Wang *et al.* [49], parameters DC in article Zhao *et al.* [46]. It contains only Acc, Se and Sp.

B. METHODS BASED ON MULTI-SCALE SEGMENTATION

Multi-scale segmentation is a method based on image characteristics at multiple levels or scales. The image is divided into rough levels, which are scales representing simplified parts of the image on a fine scale in combination with smoothing filters (e.g. Gaussian). The two most commonly used approaches for multi-scale segmentation are the pyramid and Quad-tree.

Multi-scale pyramid segmentation is based on the fact that greyscale image data is a combination of sampling operations and Gaussian smoothing filters [55]. The result of this process is a 2D Hessian matrix in which eigenvalues determine retinal blood vessels. The main directions of blood vessels can be determined by analysing the Hessian matrix. Multi-scale segmentation is suitable for structures with different widths and lengths, i.e. blood vessels [53].

A multi-scale approach to blood vessel segmentation can also be based on the superpixel division of the image into parts, which are then used as basic units to track blood vessels. A model of blood vessels is then formed by a chain of superpixel nodes. Two levels are set, which determine whether this is an area of blood vessels with good or poor imaging quality [6].

Nguyen *et al.* proposed a method based on the changing length of the line detector, which enables the detection of lines at different levels. To achieve the segmentation of blood vessels, the responses of this detector are linearly combined at different scales, thus creating a model of retinal blood vessels [52].

Abdallah *et al.* proposed the combination of multi-scale segmentation based on the eigenvectors of the Hessian matrix and an anisotropic diffusion filter to reduce image noise [54].

Moghimirad *et al.* performed multi-scale segmentation based on a 2D function to find the midpoint of blood vessels. Subsequently, these outputs are multiplied by the eigenvalues of the Hessian matrix. Blood vessels are then extracted and the radii of retinal vessels are determined [56]. Another possibility for the segmentation of blood vessels using multi-scale methods is to track small groups of pixels according to the brightness condition for whether or not it is part of the vascular system [41].

TABLE 6. Overview of methods used with results of algorithm effectivity based on region-based segmentation.

Authors	Year	Dataset (size)	Method	Measurement of algorithm effectivity
Chen et al. [45]	2016	STARE	Level Set Method	Acc = 0.94 Se = 0.74 Sp = 0.96
		DRIVE		Acc = 0.94 Se = 0.74 Sp = 0.97
Zhao et al. [46]	2015	STARE (20)	Active Contour, Infinite Perimeter	Acc = 0.96 Se = 0.78 Sp = 0.98
		DRIVE (20)		Acc = 0.95 Se = 0.74 Sp = 0.98
		VAMPIRE (8)		Acc = 0.98 Se = 0.73 Sp = 0.99
Zhao et al. [7]	2015	STARE (20)	Active Contour with Local phase	Acc = 0.95 Se = 0.79 Sp = 0.97
		DRIVE (20)		Acc = 0.95 Se = 0.74 Sp = 0.98
		ARIA (143)		Acc = 0.94 Se = 0.75 Sp = 0.93
		VAMPIRE (8)		Acc = 0.98 Se = 0.72 Sp = 0.98
Gongt et al. [47]	2015	DRIVE	Level set without using local region area	Acc = 0.94 Se = 0.71 Sp = 0.97
Zhang et al. [48]	2015	DRIVE	Correlational Open Active Contours	Acc = 0.95 Se = 0.75 Sp = 0.97
Wang et al. [49]	2015	STARE (20)	Active contours driven by Gaussian distribution	Acc = 0.94 Se = 0.76 Sp = 0.96
Salazar-Gonzalez et al. [155]	2014	STARE	Graph-cut method	Acc = 0.94
		DRIVE		Acc = 0.94
Xiao et al. [50]	2013	STARE (20)	Level set based on Bayesian method	Acc = 0.95 Se = 0.71 Sp = 0.97
		DRIVE (20)		Acc = 0.95 Se = 0.75 Sp = 0.98
Dizdaroglu et al. [51]	2012	DRIVE	Level set in terms of initialisation and edge detection	Acc = 0.94 Se = 0.72 Sp = 0.97

Table 7 below provides a complete overview of segmentation methods in the field of multi-scale segmentation for retinal blood vessel extraction. Based on the conditions specified in Section IV, the best method for retinal blood vessel extraction in this category appears to be the multi-scale approach using chain coding when applied to an HRF dataset

TABLE 7. Overview of multi-scale methods used for blood vessel segmentation.

Authors	Year	Dataset (size)	Method	Measurement of algorithm effectivity
Zhao et al. [6]	2018	DRIVE	Multi-scale superpixel chain tracking	Acc = 0.96 Se = 0.71 Sp = 0.98
		HRF – healthy images		Acc = 0.97 Se = 0.77 Sp = 0.99
		HRF – Glaucomatous		Acc = 0.97 Se = 0.75 Sp = 0.98
		HRF – Diabetic retinopathy		Acc = 0.96 Se = 0.76 Sp = 0.98
Nguyen et al. [52]	2013	DRIVE	Multi-scale line detection	Acc = 0.94
		STARE		Acc = 0.93
		REVIEW		Not specified
Rattathanapad et al. [53]	2012	DRIVE	Multi-scale based on line primitives	Not specified
Abdallah et al. [54]	2011	STARE	Multi-scale based on Anisotropic diffusion	Acc = 0.95
Budai et al. [55]	2010	DRIVE	Gaussian pyramid multi-scaling	Acc = 0.95 Se = 0.65 Sp = 0.97
		STARE		Acc = 0.94 Se = 0.76 Sp = 0.98
Moghimirad et al. [56]	2010	DRIVE	Multi-scale based on weighted medialness function	Acc = 0.97
		STARE		Acc = 0.98
Vlachos et al. [41]	2010	DRIVE	Multi-scale confidence matrix	Acc = 0.93 Se = 0.75 Sp = 0.96

with physiologically healthy images of patients according to Zhao *et al.* [6]. When applying segmentation algorithms to the DRIVE and STARE databases, the best algorithm appears to be that proposed by Moghimirad *et al.* [56] based on a multi-scale approach using the detection of the midpoint of retinal vessels.

Due to the consistency of the tables, the table below does not contain these parameters AUC in article Moghimirad *et al.* [56]. It contains only Acc, Se and Sp. ''Not specified'' was written in methods, where it was not specified parameter or authors used different evaluation parameter than Acc, Se, Sp.

C. BLOOD VESSEL SEGMENTATION BASED ON MORPHOLOGICAL OPERATIONS

Morphological operations are mathematical techniques that use image processing with the aid of geometric structures. Morphological transformations function as operators for an image set and structural element set that characterises the geometric structure [9].

Basic morphological operations include dilatation, erosion, skeletonization, closure, opening. Mathematical morphologies were traditionally applied to binary or greyscale images. These types of morphological operations can be used in image pre-processing to highlight the structure of objects of interest or applied to segment structures of interest. The principle of the algorithm is the movement of the structural element around the image according to the type of operation and the creation of new pixel values in the image [11], [58].

Methods based on morphological operations were used in this subsection. Using these geometric structures, it is possible to work with the shape of objects and image transformations, while preserving the shape of these objects.

Jadhav *et al.* applied the segmentation algorithm to artificially noisy retinal images and observed the effect of the proposed algorithm on the segmentation of retinal blood vessels with respect to different noise settings. The core of the segmentation algorithm is the application of mathematical morphology and discrete wavelet transform to a pre-processed and filtered image [57].

In another approach, the procedure was similar; the image was pre-processed and then Otsu thresholding was applied. Subsequently, the morphological opening operation removed white pixels in the image that were identified as noise. The result was segmented retinal blood vessels, with the retinal edge eliminated by the Hough transform [58].

Multiple morphological operations can be combined for retinal blood vessel segmentation in order to create a segmentation algorithm as indicated in the literature [11], [59]. Canny edge detection was applied to a pre-processed image, followed by the morphological operation of dilatation, closure, and in the final step skeletonization to form the skeleton of blood vessels [11].

In another approach, a combination of ***Top-hat transform*** and morphological erosion was used to find the optimal global threshold for retinal blood vessel segmentation [59].

Kundu *et al.* combined the morphological operations of erosion, dilation, opening, closure, top-hat transform into a method called MASS (Morphological Angular Scale-Space). The linear structural element moves around the image and determines connected pixels that are part of blood vessels. The scale is created by changing the length of the structural element [61].

Frucci *et al.* approached segmentation by division, taking into account the morphological properties of blood vessels [60]. The approach developed by Oloumi *et al.* consists of the application of a Gabor filter to detect vessels in each pixel, followed by the morphological operation open to obtain the skeleton of blood vessels [18].

Table 8 below provides a complete overview of segmentation methods based on morphological operations for retinal blood vessel extraction.

Based on the conditions specified in Section IV, the best method for retinal blood vessel extraction in this category appears to be the method proposed by Lovely *et al.* [9] based on the morphological gradient applied to the STARE

TABLE 8. Overview of segmentation methods used based on morphological operations.

Authors	Year	Dataset (size)	Method	Measurement of algorithm effectivity
Krestanova et al. [11]	2020	RetCam3 database (22)	Morphological operation (dilatation, erosion, skeletonization)	Not specified
Lovely et al. [9]	2019	DRIVE	Morphological gradient	Acc = 0.95
		STARE		Acc = 0.96
Jadhav et al. [57]	2019	DRIVE	Mathematical operation with discrete wavelet transform	Not specified
Ozkava et al.[58]	2018	DRIVE	Otsu thresholding and Morphological open	Acc = 0.96 Se = 0.85 Sp = 0.96
Kubicek et al. [38]	2018	RetCam3 database (22)	Morphological operation (dilatation, erosion, skeletonization)	Not specified
Jiang et al. [59]	2017	DRIVE	Global thresholding based on morphological operations (Top-hat transform and morphology erosion)	Acc = 0.96 Se = 0.84 Sp = 0.97
		STARE		Acc = 0.96 Se = 0.78 Sp = 0.97
Frucci et al. [60]	2014	DRIVE	Watershed transform + Contrast and directional Maps	Acc = 0.52
Oloumi et al. [18]	2014	TROPIC	Gabor filter with morphological operation open	Not specified
Kundu et al. [61]	2012	DRIVE	Morphological Angular Scale-space	Not specified

database. The best method for the DRIVE database based on the parameters Acc, Se and Sp, is the method proposed by Ozkava *et al.* [58], which is based on Otsu thresholding and morphological opening. Although the specificity of this algorithm is marked as the lowest, it differs from the highest value of specificity by 0.0072. It is marked as the lowest, because Acc was used as the primary evaluation parameter in this category, although in one case the MSE (mean square error) parameter was used for evaluation or the algorithm was not objectively evaluated at all.

Due to the consistency of the tables, the table below does not contain these parameters PPV (precision) in article Frucci *et al.* [60] and parameter MSE in article Kundu and Chatterjee [61]. It contains only Acc, Se and Sp. ''Not specified'' was written in methods, where it was not specified parameter or authors used different evaluation parameter than Acc, Se, Sp.

D. ADAPTIVE THRESHOLDING

Adaptive thresholding is a thresholding method that uses a different thresholding value for different parts of the image. This is called variable thresholding. In medical images, objects are represented by different pixel values in greyscale. The image can be divided into individual parts of the image using thresholds, each of which is characterised by greyscale pixel values with minimal noise. The threshold can be set using a global value that optimally maximises the separation between different classes in the image.

The problem with blood vessel segmentation using adaptive thresholding is uneven illumination, artefacts, noise distortion, low image resolution, and also the fine transition between shades of grey. Thresholding using one global threshold can then lead to the pixels of different objects being segmented into one anatomical object. The threshold for blood vessel segmentation can be divided into methods based on statistical elements, knowledge or fuzzy logic. In the individual approaches (see Table 9), images were pre-processed in combination with wavelet transform or filters, and subsequently adaptive thresholding was applied [62], [64].

Ali *et al.* used the well-known ***B-COSFIRE*** (Bar-selective Combination of Shifted Filter Responses) filter in combination with adaptive thresholding to achieve the binarization of retinal blood vessels. Two methods, ISODATA and Otsu thresholding were used as part of adaptive thresholding to find the optimal threshold. The combination of the B-COSFIRE filter with the ISODATA method achieved better results than the combination with Otsu thresholding [62].

Elbalaoui *et al.* applied a ***multi-scale Hessian filter*** on a pre-processed image to further highlight and extract blood vessels based on information about the image in greyscale and local geometric properties. This improved filter is based on the adaptive thresholding of blood vessels [5].

Christodoulidis *et al.* use the multi-scale detection of retinal blood vessels in combination with adaptive thresholding of the pre-processed image. The adaptive threshold value is found as:

$$T = |\mu_{Gaussian}| + \alpha\,|\sigma_{Gaussian}| \tag{1}$$

where T is the threshold value and $\mu_{Gaussian}$ a $\sigma_{Gaussian}$ are the mean and standard deviation of the Gaussian function applied to the histogram of the image [34].

Mapayi *et al.* used an algorithm based on the ***GLCM (grey level cooccurrence matrix)*** energy information of retinal blood vessels to find the local adaptive threshold [63].

Another possibility is the use of ***MCA (morphological component analysis)*** for the extraction of blood vessels, followed by the application of Morlet wavelet transform to highlight retinal vessels. The resulting model of blood vessels is created using adaptive thresholding. The threshold value is determined as 88% of the CDF (Cumulative Density Function) applied to the output of Morlet wavelet transform [44].

Fathi *et al.* used ***complex continuous wavelet transform (CCWT)*** and adaptive thresholding to highlight blood vessels. CCWT parameters are set so that linear structures are separated from the simple edges in the image in all directions. Adaptive thresholding based on the histogram of the image is then used to extract blood vessels [64]. Table 9 below

TABLE 9. Overview of adaptive thresholding used for blood vessel segmentation.

Authors	Year	Dataset (size)	Method	Measurement of algorithm effectivity
Ali e t al. [62]	2019	DRIVE	B-COSFIRE filter with adaptive thresholding	Se = 0.78 Sp = 0.97
		STARE		Se = 0.80 Sp =0.96 Acc = 0.94
Elbalaoui et al. [5]	2016	DRIVE	Adaptive thresholding with Hessian multiscale	Se = 0.76 Sp = 0.97
		STARE		Acc = 0.93 Se = 0.84 Sp = 0.95,
		CHASE_ DB1		Acc = 0.93 Se = 0.79 Sp = 0.95
Christodoulidis et al. [35]	2016	HRF	Local adaptive thresholding based on multi-scale tensor voting	Acc = 0.95 Se = 0.85 Sp = 0.96
Mapayi et al. [63]	2015	DRIVE	Adaptive Thresholding based on grey level cooccurrence matrix	Acc = 0.95 Se = 0.77
		STARE		Acc = 0.95 Se = 0.76
Imani et al. [44]	2015	DRIVE	Combination Morlet Wavelet Transform with Adaptive Thresholding	Acc = 0.95 Se = 0.75 Sp = 0.98
		STARE		Acc = 0.96 Se = 0.75 Sp = 0.97
Fathi et al. [64]	2012	DRIVE	Combination complex continuous wavelet transform with Adaptive Thresholding	Acc = 0.96 Se = 0.78 Sp = 0.98
		STARE		Acc = 0.96 Se = 0.81 Sp 0.97

provides a complete overview of segmentation methods using adaptive thresholding for retinal blood vessel extraction.

Based on the conditions specified in Section IV, the best method for retinal blood vessel extraction from images from the DRIVE and STARE databases in this category appears to be the method proposed by Fathi *et al.* [64], which is based on a combination of complex continuous wavelet transform and adaptive thresholding.

Due to the consistency of the tables, the table below does not contain these parameters PPV (precision) in article Frucci *et al.* [60] and parameter MSE in article Kundu and Chatterjee [61]. It contains only Acc, Se and Sp. ''Not specified'' was written in methods, where it was not specified parameter or authors used different evaluation parameter than Acc, Se, Sp.

E. ALGORITHMS FOR TRACKING BLOOD VESSELS

The initial step of ***vessel tracking algorithms*** is the definition of seed (starting) pixels. These seed points can be defined manually or automatically using tracking approaches. The disadvantage of manually selecting the starting pixel is that the choice of this starting pixel affects resulting image segmentation. The resulting segmentation is also affected by the order of the regions in which they are connected. Non-homogenous brightness of the image can be a problem as the region grows.

The next step is the segmentation of blood vessels, which can be achieved with a limited number of seed pixels; this is also the basic difference between the algorithms used. Models track blood vessels with minimal paths, these approaches search for the minimum path between two starting points according to metrics that are derived from the image.

The image must be pre-processed prior to vessel detection to improve vessel visibility of all vessel sizes and orientations. Vessel ridges are detected by calculating zero crossing and curvature.

The method based on mathematical graph theory is another method for tracking blood vessels [66]. Edge points can be detected iteratively based on the ***Bayesian approach*** using local grey levels and vessel properties [1], [73]. Another vessel tracking approach is tracking invertible orientation scores using Euclidean calculation [66]. The aforementioned method of minimal or geodesic path with respect to the local weight potential is used for tracking blood vessels, i.e. the connecting path between two endpoints. These methods are being improved [67], [70]–[72], [74].

Bhuivan *et al.* modified vessel ***tracking with edge profiling***, where the first or second edge of the vessel is defined to determine the direction and true width in microns using image calibration and micron calculation. In contrast to other methods, this approach takes into account the central reflex of the vessel, thus identifying the vessel with high accuracy and resolution [68].

Another approach allows particle ***filtration for local vessel tracking*** based on the probability density function in the image. The method is applied to the image after pre-processing. The optic disc is used as the initialisation point. In principle, this is about the uniform growth of particles around each, even new initialisation point. Subsequently, it is decided whether or not the particle is part of retinal blood vessels based on the value of the number of particles (weight) [69]. Table 10 below provides a complete overview of segmentation methods using algorithms for tracking retinal vessels for the purpose of their extraction.

Based on the conditions specified in Section IV, the best method appears to be the method proposed by Liao *et al.* [70], which is based on length regulation with the shortest path, which was applied to 4 images in the DRIVE database with an accuracy of up to 0.99. However, the method proposed by Kaul *et al.* [74], also based on tracking vessels with the shortest path, is also highly rated. Other parameters such as sensitivity and specificity were marked for this method. This method achieved an accuracy of 0.95, a sensitivity of 0.71 and a specificity of 0.97 for the STARE database and an accuracy

of 0.95, sensitivity of 0.75 and specificity of 0.98 for the DRIVE database.

Due to the consistency of the tables, the table below does not contain these parameters AMTR and FMTR in article Nayebifar *et al.* [69], TPR and FPR in article Yin *et al.* [1], AU ROC in article Rouchdy and Cohen [71] or without parameter by visual comparison in article Chen *et al.* [67], Li *et al.* [73], Bekkers *et al.* [66]. It contains only Acc, Se and Sp. "Not specified" was written in methods, where it was not specified parameter or authors used different evaluation parameter than Acc, Se, Sp.

F. KERNEL-BASED TECHNIQUE

The kernel-based method can be classified as machine learning. These are sorting algorithms that work on pattern analysis. The principle of this method is the creation of a filter kernel based on tracking the distribution of pixel intensities in retinal blood vessels. The filter kernel subsequently moves around the image and detects the structure of blood vessels and their boundaries, or it may be deformable according to vessel boundaries, especially if they lie in or adjacent to haemorrhages or microaneurysms.

Kernel-based techniques can be used to pre-process images so that segmentation procedures can be applied to these images. The principle of kernel-based methods is combined filtering, which compares variations in pixel intensity with the cross-sectional profiles of retinal blood vessels with a pre-set kernel. In this way, the image is filtered and undergoes thresholding. Gaussian, Laplacian of Gaussian or Gabor filter-based kernels are mostly widely used [76]–[78], [80], [83].

In this area of image segmentation, it is possible to combine several methods, which gives rise to hybrid approaches. This can be, for example, a combination of morphological operations and a combined filter based on Gaussian distribution or a combination of a Gabor filter with entropic adaptive thresholding [77], [78].

Singh *et al.* used a modified filter in combination with Gumbel probability distribution as the kernel for the detection of blood vessels. By replacing typical Gaussian distribution with Gumbel, there was higher accuracy in the detection of retinal blood vessels [75].

Zolfagharnasab *et al.* replaced Gaussian distribution with Cauchy probability distribution in the modified filter [79]. Table 11 below provides a complete overview of segmentation methods using kernel-based methods for retinal blood vessel extraction.

Based on the conditions specified in Section IV, the best method for the DRIVE database appears to be the method proposed by Villalobos-Castaldi *et al.* [83], based on a Gaussian adaptive filter with an adaptive thresholding kernel. Kumar *et al.* [76] proposed a quality segmentation algorithm for the STARE database based on a Laplacian of Gaussian filter kernel.

Kaba *et al.* proposed method based on integrating bias correction and combination matched filtering and expectation maximisation. The method expectation maximisation calculates expected value from probability function with maximalisation function. Output of the algorithm is segmentation blood vessel, because algorithm can determine which

TABLE 10. Overview of algorithms used for blood vessel tracking.

Authors	Year	Dataset (size)	Method	Measurement of algorithm effectivity
De et al. [65]	2016	DRIVE STARE	Vessel tracking using mathematical graph theory	Acc = 0.51 Acc = 0.43
Bekkers et al. [66]	2014	REVIEW	Edge tracking in orientation scores (cake wavelets) Multi-scale Vessel Centre-Line Tracking algorithm using orientation scores	Not specified
Chen et al [67]	2014	2 fundus camera images 2 magnetic resonance angiographs	Key points connected by geodesic minimal paths	Not specified
Bhuiyan et al. [68]	2013	Private database with fundus retinal images	Central Retinal Artery Equivalent Central Retinal Vein Equivalent	Acc = 0.88
Nayebifar et al [69]	2013	DRIVE STARE	Particle filters based on probability density function	Not specified Not specified
Liao et al.[70]	2013	DRIVE (4)	Length regularisation with shorter paths	Acc = 0.99
Rouchdy et al [71]	2013	ARIA (143)	Geodesic path	Acc = 0.94 Se = 0.75 Sp = 0.93
Stuhmer et al [72]	2013	DRIVE	Geodesic shortest path tree	Acc = 0.95
Li et al [73]	2013	REVIEW	Vessel tracking by Bayesian theory	Not specified
Kaul et al [74]	2012	STARE (20) DRIVE (20)	Vessel tracking with minimal path	Acc = 0.95 Se = 0.71 Sp = 0.97 Acc = 0.95 Se = 0.75 Sp = 0.98
Yin et al [1]	2012	REVIEW	Probabilistic vessel tracking	Not specified

pixels are from blood vessels and pixels which belong to background [156].

Due to the consistency of the tables, the table below does not contain these parameters ROC in article Kumar *et al.* [76], FPR in article Zolfagharnasab and Naghsh-Nilchi [79], AUC in article Odstrcilik *et al.* [80] or by fusion in article Lu *et al.* [77]. It contains only Acc, Se and Sp. ''Not specified'' was written in methods, where it was not specified parameter or authors used different evaluation parameter than Acc, Se, Sp.

G. UNSUPERVISED MACHINE LEARNING

Unsupervised machine learning methods do not work with images as samples, as is the case with supervised machine learning. Unsupervised methods use rule-based knowledge of vascular structure. These include algorithms such as matched filtering, morphological processing, multi-scale and tracking approaches. These methods have already been described above with respect to division into smaller, more comprehensive groups. This subsection contains a list of other common unsupervised methods, such as ANN (artificial neural network) [86], [90], Fuzzy C-means algorithms [41], [89], [91], [93], [94], PSO (Particle Swarm Optimisation) [39], ACO (Ant Colony Optimisation) [84] and others (see Table 12 below). As these methods do not work with gold standards, it is appropriate to use these methods for data analysis, where gold standards are not available.

In general, unsupervised learning takes place as follows: image segmentation is based on local intensity and gradient, then the model is finetuned according to a minimisation function to find the best separation of blood vessels from the retinal background. This function is usually defined based on Euclidean metrics or probability distance.

Images of blood vessels are not homogeneous; they have different brightness and contrast. For this reason, phase congruence is first performed before applying ***Fuzzy C-means***, which preserves the properties of phase frequency components such as edges in the image and suppresses other parts. The Fuzzy C-means clustering algorithm (FCM) uses language descriptions to decide whether or not an object is a blood vessel. Fuzzy tracking is based on determining the membership of functions in two language values. The optic nerve is usually used as the starting point of the algorithm. The k-means method, which uses the natural grouping of pixels in an image, can also be included in clustering algorithms. This is achieved by calculating the distances between pixels and centroids. So-called clusters are subsequently formed [41], [89], [91], [93], [94].

The fuzzy edge detector uses the method of Kubicek et al [36]. for the extraction of retinal blood vessels, which uses a combination of fuzzy logic and morphological techniques. The fuzzy edge detector detects edges and suppresses high-frequency noise in a non-contrast image. A binary model of retinal blood vessels is subsequently obtained by morphological operations [36].

TABLE 11. Overview of kernel-based algorithms used.

Authors	Year	Dataset (size)	Method	Measurement of algorithm effectivity
Singh et al [75]	2016	DRIVE	Filter Kernel: Gumbel probability Density Function	Acc = 0.93
		STARE		Acc = 0.91
Kumar et al [76]	2016	DRIVE	Filter Kernel: Laplacian of Gaussian	Acc = 0.96
		STARE		Acc = 0.96
		HRF		Acc = 0.95
Lu et al [77]	2016	DRIVE	Mathematical morphology with combination Gabor and matched filter	Not specified
Chakraborti et al [19]	2015	DRIVE	Adaptive matched filter	Acc = 0.94 Se = 0.72 Sp = 0.96
		CHASE DB		Acc = 0.93 Se = 0.54 Sp = 0.96
		STARE		Acc = 0.94 Se = 0.68 Sp = 0.96
Singh et al [78]	2015	DRIVE	Modified Gaussian matched filter + Entropy thresholding	Acc = 0.95 Se = 0.67 Sp = 0.97
Zolfagharnasab et al [79]	2014	DRIVE	Filter kernel: Caushy probability Density Function	Acc = 0.92
Odstrcilik et al [80]	2013	DRIVE	Improved t-dimensional Gaussian matched filter	Acc = 0.93 Se = 0.71 Sp = 0.97
		STARE		Acc = 0.93 Se = 0.78 Sp = 0.95
		HRF		Acc = 0.95 Se = 0.77 Sp = 0.97
Kaba et al. [156]	2013	STARE	Matched filter, Expectation maximasation	Acc = 0.95
Kaur et al [81]	2012	DRIVE	Filter Kernel, Gabor filter	Se = 0.86, Sp = 0.96
		STARE		Se = 0.85, Sp = 0.96
Zhang et al [82]	2010	DRIVE	Two kernels: Gaussian + first-order derivative of Gaussian	Acc = 0.94
		STARE		Acc = 0.94
Villalobos-Castaldi et al [83]	2010	DRIVE	Gaussian matched filter + entropy adaptive thresholding	Acc = 0.98 Se = 0.96 Sp = 0.95

Another method classed as unsupervised learning is the method of ***particle swarm optimisation (PSO).*** This is an optimisation technique with a stochastic approach, based on the behaviour of the population [39].

Another type of optimisation method used is ***the ant colony (ACO),*** which is a heuristic method. This method is based on the behaviour of ant colonies, used to solve discontinuous optimisation problems [84].

It is possible to use a combination of a Gaussian filter, Top-hat transform, morphological operations and adaptive thresholding for blood vessel segmentation as found in the literature [85]. As this is a hybrid method with multiple segmentation procedures, it was included here under unsupervised learning.

Mapayi *et al.* use the ***K-means method*** for segmentation, which is an algorithm for non-hierarchical cluster analysis [20]. Azzopardi *et al.* proposed a combination of shifted ***COSFIRE filter*** responses for subsequent detection of vascular structures [87]. Table 12 below provides a complete overview of segmentation methods in the field of unsupervised machine learning for retinal blood vessel extraction.

Based on the conditions specified in Section IV, the best segmentation method for the DRIVE and STARE databases appears to be the method proposed by Gu et al [92], which is based on an iterative classification tree.

Due to the consistency of the tables, the table below does not contain these parameters ROC in articles Roy and Sheet [86], Maji *et al.* [90], AUC in articles Azzopardi *et al.* [87], Roychowdhury *et al.* [88], Wang *et al.* [95], Lam *et al.* [97], PPV in article Gu *et al.* [92] and without specified parameter in article Xie *et al.* [41]. It contains only Acc, Se and Sp. "Not specified" was written in methods, where it was not specified parameter or authors used different evaluation parameter than Acc, Se, Sp.

TABLE 12. Overview of the use of unsupervised machine learning algorithms.

Authors	Year	Dataset (size)	Method	Measurement of algorithm effectivity
Kubicek et al. [36]	2019	RetCam3	Fuzzy Sobel Edge detection	Not specified
Asad et al. [84]	2017	DRIVE (20)	Ant Colony system	Se = 0.75
Neto et al [85]	2017	DRIVE	Coarse segmentation refined through curvature analysis and morphological reconstruction	Se = 0.78 Sp = 0.96
		STARE		Se = 0.83 Sp = 0.94
Roy et al [86]	2016	DRIVE (20)	Denoised stacked auto-encoder ANN	Not specified
Mapayi et al [20]	2016	DRIVE	K – means	Acc = 0.96 Se = 0.76
		STARE		Acc = 0.95 Se = 0.77
Azzopardi et al [87]	2015	DRIVE	Combination of Shifted Filter Responses	Acc = 0.94 Se = 0.77 Sp = 0.97
		STARE		Acc = 0.95 Se = 0.77 Sp = 0.97
		CHASE_DB1		Acc = 0.94 Se = 0.76 Sp = 0.96
Roychowdhury et al [88]	2015	DRIVE	Adaptive thresholding with global threshold with Region Grown	Acc = 0.95 Se = 0.74 Sp = 0.98
		STARE		Acc = 0.96 Se = 0.73 Sp = 0.98
		CHASE_DB1		Acc = 0.95 Se = 0.76 Sp = 0.96
Mapayi et al [89]	2015	DRIVE (20)	Fuzzy C-means and grey level co-occurrence matrix sum entropy	Acc = 0.93
		STARE (20)		Acc= 0.94
Maji et al [90]	2015	DRIVE (20)	Hybrid architecture of deep ANN	Acc = 0.93
Sreejini et al [39]	2015	DRIVE (20)	Particle swarm optimisation with Gaussian matched filter	Acc = 0.96 Se = 0.71 Sp = 0.99
		STARE (20)		Acc = 0.95 Se = 0.72 Sp = 0.97
Sharma et al [91]	2015	DRIVE (20- 30)	Fuzzy Logic Ensemble Learning	Acc = 0.95
Gu et al [92]	2015	DRIVE	Iterative Latent classification tree	Acc = 0.97
		STARE		Acc = 0.98
Akhavan et al [93]	2014	DRIVE	Vessel tracking + Fuzzy c-means	Acc = 0.73 Se = 0.97 Sp = 0.95
		STARE		Acc = 0.78 Se = 0.97 Sp = 0.95

H. SUPERVISED LEARNING ALGORITHMS AND DEEP LEARNING

Segmentation methods based on supervised learning are robust and effective when applied to image data with different image properties, even if the neural network is trained on a single database. ***The supervised machine learning method*** requires the availability of gold standards that function as a training set on which the neural network learns. The training set contains manually processed and segmented images, marked by an ophthalmologist as the gold standard. The classification criteria of images are determined by the properties of the training set.

The supervised methods were divided into two tables. Table 13 contains articles which using Convolutional neural network (CNN) algorithms and Table 14 contains articles which using supervised method as Complex-Valued Artificial Neural Network (CVANN), Pulse-coupled neural network (PCNN) AdaBoost etc. see below.

Another important group is deep learning, which is a very young field in artificial intelligence, and a subset of machine learning. It is based on multilayer neural network structures [118], [119]. The most widely used neural network for blood vessel segmentation from retinal data, which is ***CNN*** or the convolutional neural network, can be included here [98], [101], [103], [105], [111], [121], [123].

Other networks used are CVANN (Complex-Valued Artificial Neural Network) [137]. and PCNN (Pulse-coupled neural

TABLE 12. *(Continued.)* **Overview of the use of unsupervised machine learning algorithms.**

Emary et al [94]	2014	DRIVE (40)	Possibilistic version of fuzzy c-means Optimised with Cuckoo search algorithm	Acc = 0.94 Se = 0.63 Sp = 0.98
		STARE (20)		Acc = 0.94 Se = 0.59 Sp = 0.99
Zhang et al [3]	2015	DRIVE STARE	SOM (self-organising map)	Acc = 0.94
Nguyen et al [52]	2013	DRIVE	Basic line detector	Acc = 0.94
		STARE		Acc = 0.93
Xie et al [41]	2013	DRIVE (40)	Genetic Algorithm + Fuzzy c-means	Not specified
Wang et al [95]	2013	DRIVE	Multiwavelet kernels and multiscale hierarchical decomposition	Acc = 0.95
		STARE		Acc = 0.95
Yin et al [96]	2013	DRIVE	Probabilistic tracking method	Acc = 0.93 Se = 0.65 Sp = 0.97
		STARE		Acc = 0.94 Se = 0.73 Sp = 0.97
Lam et al [97]	2010	DRIVE	Line-shape concavity modelling	Acc = 0.95
		STARE		Acc = 0.96

network) [113]. CNN uses information from shallow to deep layers to determine the fine details and overall structure of retinal vessels [98], [101], [130]. An example of CNN network design might be an input convolution layer containing $1 \times 28 \times 28$ patches. The first and second layers contain 32 filters in each layer, the third and fourth contain 64 filters in each layer. The sixth layer is ascending to increase the spatial dimension of structured output. The seventh and eighth layers again contain 32 filters in each layer [103].

A ***deep neural network*** has the ability to learn a hierarchical representation of the properties of raw pixels without knowledge of the domain. It is appropriate to use 4^{th} degree Complex Wavelet Transform for blood vessel segmentation, which shows better results in combination with CVANN [137]. These complex values are inputs for CVANN; inverse CWT are implemented as outputs in this neural network for resizing and comparison with the resulting image [137].

The PCNN method is based on the fact that the pixels of blood vessels have the same intensity. The threshold value is dynamic for each pixel value. The advantage of PCNN is that postprocessing is not required, as the output is noise-free [113].

A frequently used method is ***AdaBoost (adaptive boosting),*** often in combination with random forests. This method is a learning algorithm that linearly combines classifiers during classification and thus achieves better results than the use of classifiers alone. This method is usually combined with the random forests method or is used by the authors independently. In combination with another method, it is more general and more accurate for individual models.

The random forest method is an extension of the decision trees used for classification and regression, removing instability from decision trees. The principle of this method is the random selection of indices to construct a group of trees with controlled variation [131], [141]. The AdaBoost method is also combined with an adaptive filter [112].

Zhang *et al.* use ***random forest classification*** their application for retinal images. This is a method that creates multiple decision trees during the learning process and then determines the mode of classes that are returned from individual trees [104].

Fu *et al.* used a combination of the CNN network to generate a probabilistic model of retinal vessels. In this way, the pixels are divided into parts that belong to the background of the image and those that are part of retinal blood vessels. This method is subsequently combined with CRF (conditional random fields), thus interacting with distant points [114]. The combination of the CNN network and CRF is also used by Luo *et al.* [115].

It is also possible to use a deep neural network trained in up to 400,000 samples as a classifier with pixel resolution for blood vessel segmentation [116]. Deep neural networks are also used in the literature [117]. Table 13 below provides a complete overview of segmentation methods using supervised learning for retinal blood vessel extraction.

Based on the conditions specified in Section IV, the best segmentation method for the DRIVE database appears to be the method proposed by Ceylan and Yacar [137], which is based on complex wavelet transform in combination with CVANN.

Liskowski and Krawiec [116] is the best choice for images from the STARE database, whose method is based on deep neural network learning. Although the segmentation method proposed by Li *et al.* [117] also achieves good results, based on the comparison of available objective parameters, a more suitable method is the method proposed by Mo *et al.* [105] or alternatively Guo *et al.* [101] based on the convolutional neural network. Based on objectivization parameters, these methods are on the same level as the method based on deep learning according to Liskowski and Krawiec [116].

Due to the consistency of the tables, the Table 13 below does not contain these parameters AUC in articles Soomro *et al.* [98], Hajabdollahi *et al.* [99], Chudzik *et al.* [100], Guo *et al.* [101], Sengür *et al.* [107], Feng *et al.* [109], Soomro *et al.* [111] and AU ROC parameter in articles Mo and Zhang [105], Lahiri *et al.* [106], Wang *et al.* [129], Wu *et al.* [122] and PPV in article Feng *et al.* [109] and visual comparison in article Gu *et al.* [130]. It contains only Acc, Se and Sp. "Not specified" was written in methods, where it was not specified parameter or authors used different evaluation parameter than Acc, Se, Sp.

Due to the consistency of the tables, the Table 14 below does not contain these parameters PPV in articles Orlando *et al.* [102], Zhang *et al.* [139], Marín *et al.* [140] and MCC in article Orlando et al [102], Vega *et al.* [2] and FPR in articles Francis *et al.* [113], Zhang *et al.* [139] and AUC in

TABLE 13. Overview of the use of supervised algorithms by cnn.

Authors	Year	Dataset (size)	Method	Measurement of algorithm effectivity
Soomro et al [98]	2018	DRIVE	CNN (Convolutional Neural Network)	Acc = 0.95 Se = 0.74 Sp = 0.96
		STARE		Acc = 0.95 Se = 0.75 Sp = 0.96
Hajabdollahi et al [99]	2018	STARE	Low complexity CNN	Acc = 0.96 Se = 0.78 Sp = 0.98
Chudzik et al [100]	2018	DRIVE	CNN	Se = 0.79 Sp = 0.97
		STARE		Se = 0.83 Sp = 0.98
Guo et al [101]	2018	DRIVE	Multi-scale with CNN	Se = 0.79 Sp = 0.98
		STARE		Se = 0.82 Sp = 0.98
Mo et al [105]	2017	DRIVE (20)	Fully CNN	Acc = 0.95 Se = 0.78 Sp = 0.98
		STARE (20)		Acc = 0.97 Se = 0.81 Sp = 0.98
		CHASE (20)		Acc = 0.96 Se = 0.77 Sp = 0.98
Lahiri et al [106]	2017	DRIVE (20)	CNN	Not specified
Sengür et al [107]	2017	DRIVE	CNN	Acc = 0.92
Song et al [108]	2017	DRIVE	CNN	Acc = 0.95 Se = 0.75 Sp = 0.98
Feng et al [109]	2017	DRIVE	CNN	Acc = 0.96 Se = 0.78 Sp = 0.98
Tan et al [110]	2017	DRIVE	CNN	Acc = 0.93 Se = 0.75 Sp = 0.97
Soomro et al [111]	2017	DRIVE	CNN	Acc = 0.95 Se = 0.75 Sp = 0.92
		STARE		Acc = 0.95 Se = 0.75 Sp = 0.92
Fu et al [114]	2016	DRIVE (20)	Combination CNN and Conditional Random Field	Acc = 0.95 Se = 0.76
		STARE (20)		Acc = 0.96 Se = 0.74
		CHASE (20)		Acc = 0.95 Se = 0.71
Luo et al [115]	2016	DRIVE (20)	Combination CNN with Conditional Random Field	Acc = 0.95 Se = 0.75
Khalaf et al [121]	2016	DRIVE	CNN	Acc = 0.95 Se = 0.84 Sp = 0.96
Wu et al [122]	2016	DRIVE (20)	CNN with use of PCA (Principal Component Analysis)	Not specified
Yao et al [123]	2016	DRIVE	CNN	Acc = 0.94 Se = 0.77 Sp = 0.96
Melinščak et al [127]	2015	DRIVE	Deep max-pooling CNN	Acc = 0.95 Se = 0.73 Sp = 0.98
Wang et al [129]	2015	DRIVE (20)	CNN and Random Forest	Acc =0.95 Se = 0.74 Sp = 0.98
		STARE (20)		Acc =0.95 Se = 0.75 Sp = 0.98
Gu et al [130]	2015	DRIVE	CNN	Not specified
		STARE		

articles Zhang *et al.* [104], Liskowski *et al.* [116], Strisciuglio *et al.* [126], Roychowdhury *et al.* [128], Fraz *et al.* [138], Maninis *et al.* [120] and AU ROC in articles Li *et al.* [117], Ganin *et al.* [133], Lupascu *et al.* [141] and PPV in articles Maninis *et al.* [120], Becker *et al.* [135], Marín *et al.* [140], Zhang *et al.* [139] and ROC in article Noc *et al.* [124] and F1 Score in article Vega *et al.* [2] and TPR in article Zhang *et al.* [139]. It contains only Acc, Se and Sp. ''Not specified'' was written in methods, where it was not specified parameter or authors used different evaluation parameter than Acc, Se, Sp.

I. EVALUATION OF SEGMENTATION ALGORITHMS BASED ON OBJECTIVE PARAMETERS

Objectification parameters are used to objectively evaluate the quality of the algorithms. Parameters such as Acc, Se, Sp, AUC etc. can be included here. More information about all used parameters in selected articles are described in Section V.

The effectivity or quality of the proposed segmentation algorithm for retinal blood vessel extraction can be evaluated based on objectification parameters. It is not possible to unequivocally say which of the methods described in this review is the best. This is because segmentation algorithms were tested on different datasets (see Section IV) with different numbers of images or different objectivization parameters were used to evaluate algorithms.

Nevertheless, the two tables below list the ten best rated segmentation algorithms based on the Acc parameter (see Table 15) and the AUC parameter (see Table 16). These parameters were most widely used in objective evaluations of the proposed algorithms.

Based on Table 15, it can be said that the best method for blood vessel extraction is the method based on tracking vessels using the shortest path. This method was applied to a DRIVE dataset with 4 images with an Acc accuracy of 0.99 [70]. The segmentation algorithms in Table 15 come from different groups such as: supervised learning [105], [116], [137], region-based deformable methods [7], unsupervised machine learning [9], kernel-based algorithms [83], and multi-scale segmentation [56].

TABLE 14. Overview of the use of algorithms for supervised learning and deep learning.

Authors	Year	Dataset (size)	Method	Measurement of algorithm effectivity
Orlando et al [102]	2017	DRIVE (20) STARE (20) CHASED B1 (20) HRF (20)	Fully connected conditional random field model	Se = 0.79 Sp= 0.97 Se = 0.77 Sp = 0.97 Se = 0.73 Sp = 0.97 Se = 0.79 Sp = 0.96
Dasgupta et al [103]	2017	DRIVE (20)	Convolutional ANNs	Acc =0.95 Se = 0.75 Acc=0.95
Zhang et al [104]	2017	DRIVE STARE CHASE	Random Forest classifier with wavelet transformation	Se = 0.79 Sp = 0.97 Acc = 0.95 Se = 0.79 Sp = 0.97 Acc = 0.95 Se = 0.76 Sp = 0.97
Memari et al [113]	2017	DRIVE STARE CHASE_ DB	Matched filter and AdaBoost classifier	Acc = 0.97 Acc = 0.95 Acc = 095
Francis et al [112]	2016	DRIVE	PCNN	Not specified
Liskowski et al [116]	2016	DRIVE (20) STARE (20) CHASE (28)	Deep ANNs	Acc = 0.95 Se = 0.75 Sp = 0.98 Acc = 0.97 Se = 0.82 Sp = 0.99 Not specified
Li et al [117]	2016	DRIVE (20) STARE (20) CHASE (28)	Deep ANN with cross modality	Acc = 0.96 Se = 0.76 Sp = 0.98 Se = 0.77 Sp = 0.98 Acc = 0.96 Acc = 0.96 Se = 0.75 Sp = 0.98
Javidi et al [8]	2016	DRIVE (20) STARE (20)	Discriminative dictionary learning	Acc = 0.94 Se = 0.72 Sp = 0.97 Acc = 0.95 Se = 0.78 Sp = 0.96
Fu et al [118]	2016	DRIVE STARE	Fully connected conditional random fields and deep learning	Acc = 0.95 Se = 0.76 Acc = 0.96 Se = 0.74
Lahiri et al [119]	2016	DRIVE	Deep neural network	Acc = 0.95
Maninis et al [120]	2016	DRIVE STARE	Deep Convolutional ANNs	Not specified
Noc et al [124]	2016	DRIVE (20)	Ensemble of 12 convolutional	Acc = 0.95
Aslani et al [125]	2016	DRIVE STARE	Random forest classifier trained with 17-D hybrid feature vector	Acc = 0.95 Acc = 0.96
Strisciuglio et al [126]	2016	DRIVE STARE	SVM classifier for B-COSFIRE filters	Acc = 0.95 Se = 0.78 Sp = 0.97 Acc = 0.95 Se = 0.81 Sp = 0.97
Vega et al [2]	2015	DRIVE (20)	Lattice Neural Network with Dendritic Processing	Acc=0.96 Se = 0.84 Sp=0.97
Roychowdhury et al [128]	2015	DRIVE STARE CHASE	Gaussian mixture model	Acc = 0.95 Se = 0.73 Sp = 0.98 Acc = 0.95 Se = 0.77 Sp = 0.97 Acc = 0.95 Se = 0.72 Sp = 0.98
Zhu et al [131]	2015	DRIVE	Adaboost classifier	Acc = 0.95 Se = 0.83 Sp = 0.96
Fraz et al [132]	2014	CHASE_ DB1	Ensemble classifier of bootstrapped decision trees	Acc= 0.96 Se = 0.74 Sp = 0.98
Ganin et al [133]	2014	DRIVE (20)	Neural network nearest neighbour	Not specified
Orlando et al [134]	2014	DRIVE (20)	Fully Connected CRF	Se = 0.79 Sp = 0.97
Becker et al [135]	2013	DRIVE (20)	Gradient Boosting framework for learning convolutional filter	Not specified
Chakravarty et al [136]	2013	RET-TORT	Quadratic polynomial decomposition	Not specified
Ceylan et al [137]	2013	DRIVE	Complex Wavelet Transform and CVANN	Acc = 0.99
Fraz et al [138]	2012	CHASE_ DB1 DRIVE STARE	Bagged and boosted decision tree	Acc= 0.95 Se = 0.72 Sp = 0.97 Acc = 0.95 Se = 0.71 Sp = 0.98 Acc = 0.95 Se = 0.76 Sp = 0.98
Zhang et al [139]	2012	DRIVE (20) STARE (20)	Dictionary Learning with Sparse Representation Classifier	Not specified
Marín et al [140]	2011	DRIVE (40) STARE (20)	Neural network with 7-D vector composed of grey-level and moment invariants	Acc = 0.94 Se = 0.71 Sp = 0.98 Acc = 0.95 Se = 0.69 Sp = 0.98
Lupascu et al [141]	2010	DRIVE (20)	41-D feature vector based on AdaBoost Classifier	Acc = 0.96 Se = 0.67 Sp = 0.99

The datasets in which the highest Acc values were achieved are also different. The best results for blood vessel segmentation algorithms were obtained with the DRIVE [9], [56], [70], [83], [137], VAMPIRE [7] and STARE [9], [56], [105], [116] datasets. This is also due to the fact that the DRIVE and STARE databases are the most widely used databases in the field of retinal blood vessel segmentation (see Fig. 2).

It is also evident from the table that the method based on unsupervised machine learning according to Gu et al [9] produced good results for the STARE database with Acc = 0.9772 and for the DRIVE database with 0.9732. However, on comparison, the method proposed by Liao *et al.* [70] still appears to be the best method with regard to the DRIVE database based on the Acc value.

Table 16 shows the evaluation of algorithms for retinal blood vessel segmentation based on the objective AUC parameter. The table shows that based on the AUC parameter, the best methods for blood vessel segmentation are those based on supervised learning, which involves deep neural network learning [116], convolutional neural networks [100], [101], [105], [109], [117], [127] and classification based on decision and random trees [104], [138].

The method based on unsupervised machine learning is in ninth place [96]. Segmentation algorithms were rated best for STARE, DRIVE and CHASEDB1 datasets. This is also due to the fact that the DRIVE and STARE databases are the most widely used databases in the field of retinal blood vessel segmentation (see Fig. 2).

The method proposed by Mo *et al.* based on the convolutional network has good AUC results with values of 0.99 for the STARE database and the method based on deep learning proposed by Li *et al.* also has an AUC value of 0.99 for the DRIVE database. Since the differences between the first 6 methods are in the order of thousandths, and even taking into account that the method proposed by Mo *et al.* [105] and Li *et al.* [117] has a value of 0.99, it can be said that when rounded off to hundredths, the methods in 1st to 3rd place are at the same level, because they also have an AUC value equal to 0.99. Therefore, it is necessary to compare other objectivization parameters such as Se, Sp and Acc in addition to this parameter to select the best algorithm. However, as already mentioned, this parameter implies that methods based on supervised learning are among the best segmentation algorithms for retinal blood vessel extraction.

Table 17 provides an overview of the best selected methods in each defined segmentation group in Section IV. Parameter values with the highest value are marked in green for database STARE and DRIVE. The best methods for images from the DRIVE database are the methods proposed by Liao *et al.* [70] based on vessel tracking, Ceylan *et al.* [137] based on CVANN and Villalobos-Castaldi *et al.* [83] based on kernel algorithms. These methods are highlighted below in yellow. The best methods for images from the STARE database are the methods proposed by Mo *et al.* [105] based

TABLE 15. Evaluation of segmentation methods for retinal blood vessel extraction based on the ACC parameter.

Ranking based on Acc	1. Liao et al [70]	2. Ceylan et al [137]	3. Zhao et al [7]	4. Gu et al [9]	5. Villalobos-Castaldi et al [83]	6. Moghimirad et al [56]	7. Gu et al [9]	8. Mo et al [105]	9. Liskowski et al [116]	10. Moghimirad et al [56]
Subsection	Tracking blood vessels (subsection IV. E)	Supervised learning (subsection IV. H)	Region-based deformable models (subsection IV. A)	Unsupervised learning (subsection IV. G)	Kernel-based algorithms (subsection IV. F)	Multi-scale segmentation (subsection IV. B)	Unsupervised learning (subsection IV. G)	Supervised learning (subsection IV. H)	Supervised learning (subsection IV. H)	Multi-scale segmentation (subsection IV. B)
Method	Length regularization with shorter paths	Complex Wavelet Transform and CVANN	Active Contour with Local phase	Iterative Latent classification tree	Gaussian matched filter + entropy adaptive thresholding	Multi-scale based on weighted medialness function	Iterative Latent classification tree	Fully CNN	Deep ANNs	Multi-scale based on weighted medialness function
Dataset	DRIVE	DRIVE	VAMPIRE	STARE	DRIVE	STARE	DRIVE	STARE	STARE	DRIVE
Year	2013	2013	2015	2015	2010	2010	2015	2015	2016	2010
Acc	0.99	0.99	0.98	0.98	0.98	0.98	0.97	0.97	0.97	0.97
Se	-	-	0.72	-	0.97	-	-	0.81	0.82	-
Sp	-	-	0.98	-	0.95	-	-	0.98	0.99	-

on a convolutional network and the method proposed by Liskowski *et al.* [116]. The method proposed by Gu *et al.* [93] based on unsupervised learning is also suitable for the STARE database.

Table 18 shows overview of the best segmentation algorithms from the mostly used databases DRIVE and STARE for the purpose of retinal blood vessel extraction.

V. OBJECTIVIZATION PARAMETERS FOR EVALUATION OF THE QUALITY OF SEGMENTATION ALGORITHMS

Objectification parameters are used for objectively determine quality or effectivity of proposed algorithms. The most common parameters for evaluating the effectivity of segmentation algorithms are sensitivity, specificity, accuracy, ROC curve, AUC, MSE, MCC, DSC, PPV, F1 score, AMTR and FMTR. Articles that use subjective evaluation of the quality of the algorithm based on a visual comparison of the images were also noted. The following text presents a general description of the most frequently used metrics used for the objectivization of the segmentation process.

It is not possible to unequivocally determine which type of algorithm has the best results for blood vessel segmentation, as the articles presented herein do not unequivocally agree on the system for evaluating algorithms. Some authors use a group of evaluation parameters, others only one parameter to evaluate the quality of the algorithm.

A. ACCURACY (ACC), SENSITIVITY (SE), SPECIFICITY (SP), PRECISION

Accuracy is a metric for measuring the performance of algorithms. Accuracy is calculated based on the following formula:

$$Acc = \frac{TP + TN}{(TP + FN + FP + TN)}, \tag{2}$$

where TP represents the number of objects that were classified as true positive, TN as true negative, FP as false positive, and FN as false negative [48], [105], [109].

Specificity is a metric that represents the algorithm's ability to detect background pixels, i.e., pixels other than a vessel pixel. It represents the relative success of the classification of negative TNR cases (true negative rate) [48]. It is calculated using the following formulas:

$$Sp = \frac{TN}{TN + FP} \tag{3}$$

$$Sp = 1 - FPR, \tag{4}$$

where FPR represents a false positive rate, which is given by the following formula:

$$FPR = \frac{FP}{FP + TN} \tag{5}$$

Sensitivity represents the relative success in correctly classifying objects as positive cases [48], [105], [109]. Algorithm sensitivity represents the ability to detect blood vessel pixels. Sensitivity is calculated as follows:

$$Se = \frac{TP}{TP + FN} \tag{6}$$

TABLE 16. Evaluation of segmentation algorithms for retinal blood vessel extraction based on the AUC parameter.

Ranking based on AUC	Subsection	Method	Dataset	Year	AUC
1. Mo et al [105]	Supervised learning (subsection IV. H)	Fully CNN	STARE	2017	0.99
1.Li et al [117]		Deep ANN with cross modality	DRIVE	2016	0.99
1. Liskowski et al [116]		Deep ANNs	STARE	2016	0.99
2. Guo et al [101]	Supervised learning (subsection IV. H)	Multi-scale with CNN	STARE	2018	0.99
3. Chudzik et al [100]	Supervised learning (subsection IV. H)	CNN	STARE	2018	0.98
4. Guo et al [101]	Supervised learning (subsection IV. H)	Multi-scale with CNN	DRIVE	2018	0.98
5. Feng et al [109]	Supervised learning (subsection IV. H)	CNN	DRIVE	2017	0.98
6. Melinščak et al [127]	Supervised learning (subsection IV. H)	Deep max-pooling CNN	DRIVE	2015	0.98
7. Fraz et al [138]	Supervised learning (subsection IV. H)	Bagged and boosted decision tree	DRIVE	2012	0.98

TABLE 16. *(Continued.)* **Evaluation of segmentation algorithms for retinal blood vessel extraction based on the AUC parameter.**

8. Zhang et al [104]	Supervised learning (subsection IV. H)	Random Forest classifier with wavelet transformation	STARE	2017	0.97
9. Lam et al [96]	Unsupervised learning (subsection IV. G)	Line-shape concavity modelling	STARE	2010	0.97
10. Fraz et al [138]	Supervised learning (subsection IV. H)	Bagged and boosted decision tree	CHASE_DB1	2012	0.97

The higher the value of specificity or sensitivity, the better the diagnosis can be classified. This is the most commonly used metric for evaluating algorithms [48], [105], [109].

$$FP = 1 - Sp \tag{7}$$

Precision (PPV) is a metric that indicates how many objects are actually correct with respect to the positive class only. Precision is also called PPV (positive predictive value). It is defined using the following formula [109]:

$$PPV = \frac{TP}{TP + FP} \tag{8}$$

B. RECEIVER OPERATING CHARACTERISTIC CURVE (ROC), AUC (AREA UNDER CURVE)

This parameter represents a curve that is the nonlinear function between TPR and FPR. The optimal area under the curve is 1.

The ROC curve shows the relationship between specificity and sensitivity. The evaluation of ROC curves is performed on the basis of the area under ***AUC curves*** (AU ROC), which reflect their shape by their value. ROC curves show the ability of algorithms to assign a property to specific objects with respect to whether or not they have this property. The x-axis shows FPR and the y-axis TPR values [75], [113].

C. MSE (MEAN SQUARED ERROR)

The mean square error represents a metric that compares two images. Image x after the application of a new algorithm is compared against image y defined as the gold standard. This metric is used to determine the accuracy of segmentation.

The smaller the MSE value, the greater the agreement between the images. For a two-dimensional image, MSE

TABLE 17. **Overview of best selected segmentation methods in individual segmentation groups (chapters iv. A to G).**

Author	Subsection	Method	Dataset	Year	Parameter
Zhao et al [46].	Region-based deformable models (subsection IV. A)	Active Contour, Infinitive Perimeter	VAMPIRE DRIVE STARE	2015	Se = 0.73 Se = 0.74 Se = 0.78 Sp = 0.99 Sp = 0.98 Sp = 0.98 Acc = 0.98 Acc = 0.95 Acc= 0.96 AU ROC = 0.86 AU ROC = 0.8 AU ROC =0.87 DC = 0.74 DC = 0.78 DC = 0.80
Zhao et al [6]	Multi-scale segmentation (subsection IV. B)	Multi-scale superpixel chain tracking	DRIVE HRF – healthy images	2018	Acc = 0.97 Acc =0.96 Acc =0.97 Se = 0.77 Se = 0.71 Se = 0.77 Sp = 0.99 Sp = 0.98 Sp = 0.99
Moghimirad et al [56]	Multi-scale segmentation (subsection IV. B)	Multi-scale based on weighted medialness function	STARE DRIVE	2010	Acc = 0.98 Acc = 0.97 AUC =0.96 AUC =0.97 = 0.96
Lovely et al [9]	Morphological operations (subsection IV.C)	Morphological gradient	STARE	2019	Acc = 0.95
Ozkava et al [58]	Morphological operations (subsection IV. C)	Otsu thresholding and Morphological open	DRIVE	2018	Acc = 0.96 Se = 0.85 Sp = 0.96
Fathi et al [64]	Adaptive thresholding (subsection IV. D)	Combination complex continuous wavelet transform with Adaptive Thresholding	DRIVE	2012	Acc =0.96 Acc = 0.96 Se = 0.81 Se = 0.78 Sp 0.97 Sp = 0.98

TABLE 17. *(Continued.)* **Overview of best selected segmentation methods in individual segmentation groups (chapters iv. A to G).**

Ceylan et al [137]	Liskowski et al [116]	Mo et al [105]	Guo et al [101]	Gu et al [92]		Villalobos-Castaldi et al [83]	Kumar et al [76]	Kaul et al [74]	Liao et al [70]	
Supervised learning (subsection IV. H)	Supervised learning (subsection IV. H)	Supervised learning (subsection IV. H)	Supervised learning (subsection IV. H)	Unsupervised learning (subsection IV. G)		Kernel algorithms (subsection IV. F)	Kernel algorithms (subsection IV. F)	Vessel tracking (subsection IV. E)	Vessel tracking (subsection IV. E)	
Complex Wavelet Transform and CVANN	Deep ANNs	Fully CNN	Multi-scale with CNN	Iterative Latent classification tree		Gaussian matched filter + entropy adaptive thresholding	Filter Kernel: Laplacian of Gaussian	Vessel tracking with minimal path	Length regularisation with shorter paths	
DRIVE	STARE	STARE	STARE	STARE	DRIVE	DRIVE	STARE	DRIVE	STARE	DRIVE (4)
2016	2016	2017	2018	2015		2010	2016	2012	2013	
Acc = 0.99	Se = 0.82 Sp = 0.99 Acc = 0.97 AUC = 0.99	AU ROC=0.99 Acc = 0.97 Se = 0.81 Sp = 0.98	AUC =0.99 Acc = 0.95 Se = 0.78 Sp = 0.98	Precision=0.84 Acc = 0.98	Precision =0.80 Acc = 0.97	Acc = 0.98 Se = 0.97 Sp = 0.95	Acc = 0.96 ROC = 0.96	Acc = 0.95 Se = 0.75 Sp = 0.98	Acc = 0.95 Se = 0.71 Sp = 0.97	Acc = 0.99

TABLE 18. **Overview of the best segmentation algorithms for images from the drive and stare databases for the purpose of retinal blood vessel extraction.**

Author	Liskowski et al [116]	Mo et al [105]	Gu et al [93]	Ceylan et al [137]	Villalobos-Castaldi et al [83]	Liao et al [70]
Subsection	Supervised learning. H)	Supervised learning (subsection IV. H)	Supervised learning (subsection IV. G)	Supervised learning (subsection IV. H)	Kernel algorithms (subsection IV. F)	Vessel tracking (subsection IV. E)
Method	Deep ANNs	Fully CNN	Iterative Latent classificati on tree	Complex Wavelet Transform and CVANN	Gaussian matched filter + entropy adaptive thresholding	Length regularisati on with shorter paths
Dataset	STARE	STARE	STARE	DRIVE	DRIVE	DRIVE (4)
Year	2016	2017	2015	2016	2010	2013
Parameter	Se = 0.82 Sp = 0.99 Acc = 0.97 AUC=0.99	AU ROC = 0.99 Acc = 0.97 Se = 0.81 Sp = 0.98	Precision=0.84 Acc = 0.98	Acc = 0.99	Se = 0.97 Sp = 0.95 Acc = 0.98	Acc = 0.99

calculation is defined as:

$$MSE = \frac{1}{MN} \sum_{i=1}^{M} \sum_{j=1}^{N} \left(X_{i,j} - Y_{i,j}\right)^2, \tag{9}$$

where $X_{i,j}$ and $Y_{i,j}$ represent the pixel values of two different images in one colour scale with dimensions MxN. The difference between image X and Y represents the error signal [8].

D. MATTHEWS CORRELATION COEFFICIENT (MCC)

The MCC metric is a correlation coefficient that is determined between the output image after segmentation and the binary images defined as the gold standard. Values of the correlation coefficient range between -1 and +1, where +1 indicates a perfect match between images and -1 a complete mismatch between images. MCC is calculated from the following relationship [126]:

$$MCC = \frac{(TP * TN) - (FP * TN)}{\sqrt{((TP + FP)\,(TP + FN)\,(TN + FP)\,(TN + FN))}} \tag{10}$$

E. F_1 SCORE

This is a metric for measuring an accuracy test. It takes a value from 0 to 1. Where 1 represents the best accuracy and 0 the worst. It is calculated from the following relationship [104]:

$$F_1 Score = 2.\left(\frac{PPV\,.Sensitivity}{PPV + Semsitivity}\right) \tag{11}$$

F. DSC (DICE SIMILIRATY COEFFICIENT)

The DSC (DC) coefficient is a metric for determining the similarity of images. The DSC value ranges from 0 to 1, where a value of 0 indicates there is no spatial overlap between the two images after binary segmentation and a value of 1 represents a complete overlap of images. It is calculated using the following formula [142]:

$$DSC = \frac{2TP}{2TP + FP + FN} \tag{12}$$

G. AMTR AUTOMATIC/MANUALLY TRACKED RATIO

The AMTR metric expresses the ratio of the number of tracked pixels to the number of pixels in the skeletonised image after manual segmentation. It is expressed by the following formula [69]:

$$AMTR = \frac{trackedpixels}{numberofpixels} \tag{13}$$

H. FMTR FALSE/MANUALLY TRACKED RATIO

The FMTR metric represents the ratio of the number of falsely tracked pixels to the number of pixels in a skeletonised image after manual segmentation. The formula for calculating the FMTR is [69]:

$$FMTR = \frac{falselytrackedpixels}{numberofpixels} \tag{14}$$

VI. PARAMETERS FOR MEASURING TORTUOSITY

Tortuosity, or vessel curvature, is a type of vascular pathology. This is one of the important parameters for determining the presence and severity of various diseases [36]. It affects both arteries and veins, with slight curvature of blood vessels without clinical symptoms commonly observed in both humans and animals [21]. It is also found, for example, in brain tissue, carotid arteries, skeletal muscles and retinal vessels. Vascular tortuosity is associated with atherosclerosis, retinopathy of prematurity, diabetic retinopathy, but is also found in people with high blood pressure, but also occurs naturally with age [21].

The most common forms of tortuosity includes curvatures, twists, kinks, and loops. Tortuosity is assessed by ophthalmologists manually using a contour gauge or visual comparison of images. There is no standardised metric for measuring the degree of curvature or tortuosity [21]. Scientific publications dealing with the measurement of tortuosity using metrics for the classification of blood vessel curvature are analysed below. Metrics were applied with the aim of measuring tortuosity automatically. However, metrics do not always coincide with the clinical concept of tortuosity [4]. Tortuosity metrics were applied to binary segmented images.

Onkaew *et al.* [4] approached the calculation of curvature based on the definition of the curve in Euclidean space, where the curve is defined as $y = f(x)$, while the curvature at each point $p(x, y) \in R^2$. In this way, the segmented image of blood vessels is divided into parts based on the aforementioned chain code and the degree of curvature is calculated (see Table 19).

An ophthalmologist determined whether or not there was tortuosity and then the proposed algorithm calculated the tortuosity and determined whether or not there was tortuosity based on the threshold. There was agreement between the prediction and gold standard in 8 training images [4].

Another possible metric of tortuosity is the tortuosity index, which is calculated by combining the length of the chord, the length of the arc and the frequency of vascular curvatures using stationary points. These points are determined using the gradient vector. The presence of curvature is subsequently detected by comparing the curvature samples to skeletonised blood vessels. The tortuosity index TI is then calculated. The non-normalised metric TI_{freq2} has a stronger correlation than TI_{freq1} [20].

Tortuosity is a relative feature of the vascular segment and depends on its width. For this reason, Bhuyian *et al.* also took into account the width of the vascular segment when calculating tortuosity, as tortuosity affects narrower vessels more often than wider ones.

After blood vessel segmentation, the midpoint of the vessel is determined and fragmented at the bifurcation and branching points to form individual vascular segments. The tortuosity of the vascular segment is calculated at its edge. The result is the average twist angle of the vessel segment. The accuracy of tortuosity measurements using this method was 100%, which was determined qualitatively in relation to images classified by ophthalmologists [152].

Dougherty *et al.* evaluated the proposed calculation of tortuosity using Spearman's rank correlation coefficient between calculated tortuosity and tortuosity evaluated by experts. This coefficient had a value of 0.996 on the 95% confidence interval for the M metric and 0.957 on the 95% confidence interval for the K metric (see Table 19) [153].

Makkpati *et al.* evaluated the proposed metric for determining tortuosity using the Spearman coefficient with a value of 0.8901 [143].

Continuous curves need to be discretised in order to determine the degree of tortuosity using SCC (Slope Chain Code). The calculation of tortuosity is based on the definition of the curve as the absolute value of the rate of change in the slope with respect to the tangent and distance along the curve. The convexity and concavity of curves is determined by the total slope Acc and tortuosity τ [147].

Oloumi *et al.* used the application of branch points on binary blood vessels to evaluate tortuosity. Skeletonised blood vessels are divided into segments and the AVI (Angle Variation Index) is calculated in each segment, which is based on the Gabor angle. The sum of the AVI values gives the AVT tortuosity metric that takes a value from 0 to 1 in each pixel. Retinal images are divided into normal, abnormal and plus based on the AVT parameter. The results are also distinguished by colour coding, red representing plus disease, an abnormal tortuosity value insufficient to determine plus disease in yellow, normal and low-level tortuosity in green [18].

Turior *et al.* based their method on the calculation of curvature using integration and difference. Tortuosity is then automatically classified using the Naive Bayesian classifier, the KNN classifier and the K-means clustering algorithm [148].

The most common metric of the tortuosity index is the ratio between the length of the vessel curve to the direct distance between the two ends. This metric is only amended and modified in order to more accurately measure the curvature of blood vessels. Tortuosity can further be defined as the total tortuosity or mean curvature, which is calculated as the sum of the angles between vessel segments according to the length of the vessel (see Table 19).

TABLE 19. Overview of the methods and calculations of vascular tortuosity in retinal images.

Authors	Year	Dataset (size)	Method or metric
Kubicek et al. [36]	2019	RetCam database	Calculation of curvature based on vessel gradient at each point
Mapayi et al [20]	2016	DRIVE, STARE	Arc-chord ratio and stationary points
Makkapati et al [143]	2015	Private dataset	Metrics based on Euclidean distance
Oloumi et al [18]	2014	TROPIC	Measurement based Gabor angle in each segment of curvature
Lisowska et al [144]	2014	RET-TORT	Curvature-integral measures with multiple window
Khdhair et al [145]	2013	Drawing lines	Arc to chord ratio
Mohsenin et al [146]	2013	Retinal images taken by Topcon	Arc-chord ratio
Chakravarty et al [136]	2013	RET-TORT	Absolute Direction Angle Change
Bribiesca et al. [147]	2013	Not specified	Measurement tortuosity based on Slope Chain Code
Turior et al [148]	2012	Private dataset 45 images taken by RetCam 130	Numerical Integration for determinate value of curvature
Zepeda-Romero et al. [149]	2011	Retinal images taken by RetCam II	Numerical Differentiation Method Ratio radians and pixel
Ghadiri et al. [150]	2011	DRIVE	Circular Hough Transform
Tam et al [151]	2011	AOSLO retinal images	Ratio of total squared curvature and chord length
Turior et al [10]	2011	Simulated curves	PCA (principal component analysis)
Onkaew et al [4]	2011	18 retinal images	Measurement tortuosity based on improved chain code
Bhuiyan et al [152]	2010	STARE	Total curvature
Dougherty et al [153]	2010	322 Retinal images taken by TopCon TRC-50DX	Mean tortuosity (M) and Normalized root-mean square tortuosity (K)
Joshi et al [154]	2010	15 fundus retinal images with facioscapulohumeral muscular dystrophy	Combination arc-chord ratio with angle of curvature

VII. DISCUSSION

Most articles deal with diabetic retinopathy, but only 3 articles dealt with retinopathy of prematurity [11], [18], [36]. An overview of the diseases found in retinal databases is shown in Fig. 1 for illustration. There is wide scope for research in the field of blood vessel segmentation from retinal images. It is important to address this issue, as early detection and treatment of retinopathy of prematurity allows premature infants to have physiologically healthy retinal vessels. If neglected, the disease can lead to blindness.

An important indicator is tortuosity, which can help ophthalmologists classify the severity of ROP disease and its early detection with an automatic algorithm. Testing the effectivity of algorithms applied to RetCam images is not possible, as there is no database with a gold standard for objective evaluation.

Objective comparisons for methods that do not have a gold standard is difficult to evaluate against other segmentation

procedures applied to data with a gold standard. In contrast to images from a fundus camera used to capture the retina of adults and older children, images from RetCam have lower resolution, contrast and contain more artefacts due to the insufficient development of the child's choroid, the presence of choroidal vessels and movement of the child's eyes.

For this reason, it is not possible to apply existing one-to-one segmentation algorithms that work on images from fundus cameras. However, these must be modified for use on retinal images from RetCam or they must be approached innovatively, as there are no gold standards on which techniques such as supervised learning can be trained.

In the contrast with many other reviews of retinal blood vessels such is [157], [160], this review is aimed to provide an extensive view to present the retinal blood vessels segmentation in a broader manner. Besides the segmentation algorithms, which are often a subject of other reviews, we provide an extensive investigation of available retinal databases, which are frequently used for the testing and evaluation of segmentation methods. Also, we present the methods for tortuosity extraction, which is the further step after the image segmentation, which enables quantification of the retinal blood vessels curving. Therefore, such methods have a substantial importance for the clinical ophthalmologic practice in diagnosis ROP.

VIII. CONCLUSION

This review presents an overview of segmentation techniques used to extract blood vessels from retinal images over the last 10 years, i.e. from 2010 to the present. The review includes an overview of 18 databases with retinal images, which are both public and private.

These databases are used for the application of segmentation algorithms for the segmentation of retinal blood vessels. The databases were created in collaboration with hospitals, with retinal images of adults and older children taken with a fundus camera and retinal images of young children and newborns taken with a RetCam fundus camera. The images in the databases have different resolutions, as they were taken with different types of cameras (see Table 3 and Table 4).

Diabetic retinopathy was the most frequently diagnosed disease in the databases (Fig. 1). The most widely used databases for segmentation algorithms were the open access DRIVE and STARE databases (see Fig. 2). Images from these databases have a resolution of 768 × 584 and 650 × 700 pixels and gold standards, thanks to which the effectivity of the proposed algorithms can be compared [12], [23].

Prior to the application of segmentation procedures, the authors first pre-processed retinal images in order to highlight blood vessels and suppress unwanted noise and objects. Segmentation methods for vessel extraction were then applied to these modified images based on the principle of segmentation, namely region-based deformable models, multi-scale segmentation, tracking approaches, edge-based deformable models, adaptive thresholding, supervised learning and unsupervised machine learning (Table 5). These areas represent larger groups into which segmentation methods were divided on the principle by which they detected retinal blood vessels.

Segmentation algorithms were evaluated objectively using objectivization parameters. The selection of the best method for the extraction of retinal blood vessels was hampered by certain limitations, in particular the diversity of databases on which the algorithms were tested and the variety of objective parameters used. The authors most often chose the following parameters for objective evaluation of the quality of algorithms: specificity, sensitivity and accuracy or AUC. An overview of the objectivization parameters used with their description is given in Chapter V.

The values of all parameters are given in the tables for segmentation algorithms (see Table 6 to Table 13). Another limitation in determining the best method is that some authors did not use objectivization parameters at all, because their datasets did not have gold standards, so they could not evaluate the proposed algorithm or did not specify them [11], [18], [38], [57]. The quality of the algorithm is also influenced to some extent by the size of the dataset and the composition of this dataset, whether contrast images or images with artefacts were used, etc.

The authors used different sizes of datasets with several to dozens, but also hundreds of images. This depended on the choice of sample and on the size of the source database used, although some authors did not mention the size of the dataset in the article [70], [133], [136]. The images in databases differ in terms of the number of images, image quality, resolution, contrast, brightness, and artefacts (see Table 3, Table 4).

The most effective segmentation approach for blood vessel extraction was chosen for each defined group based on a comparison of the identified objectivization parameters. Quality was determined on the basis of Acc, Sp and Se, or AUC as these were the most frequently used parameters. Those methods that did not indicate an objectivization parameter, or this differed, were not taken into account. For greater clarity in determining quality algorithms, objectivization parameters for the DRIVE and STARE databases were compared, as they were the most widely used sources. In this way, the conditions for determining the best segmentation approach were set. Selected segmentation approaches were colour-coded directly in the tables (see Table 6 to Table 14).

Table 15 and Table 16 were created for greater clarity. Table 15 shows ratings based on the Acc parameter and Table 16 based on the AUC parameter. Based on the Acc parameter, the best method for blood vessel extraction appears to be the method based on vessel tracking using the shortest path. This method was applied to a DRIVE dataset with 4 images with an Acc accuracy of 0.99 [70]. Table 17 also contains algorithms from different segmentation approaches.

The best methods for the segmentation of retinal blood vessels based on the AUC parameter are supervised learning methods, namely deep neural network learning [116], convolutional neural networks [100], [101], [105], [109], [117],

[127] and classification based on decision and random trees [104], [138]. The first 6 methods only differ in the order of thousandths, and after rounding off to hundredths, all AUC are equal to 0.99 (see Table 16).

Due to the small difference in AUC values, the parameters Acc, Sp and Se must be taken into account in order to determine the best algorithm.

Table 17 provides an overview of the best selected methods for each segmentation group. This table shows that the following methods are best for images from the DRIVE database:

- Ceylan et al [137] – method based on complex wavelet transform and CVANN
- Villabos-Castaldi et al [83] – method based on kernel algorithms
- Liao et al [70] – method based on vessel tracking

The best methods for images from the STARE database were:

- Mo et al [105], Liskowski et al [116] – method based on convolutional networks
- Gu et al [93] – method based on an iterative classification tree

The metric for measuring tortuosity is most often based on the ratio of the length of the arc (curve) to the length of the cut, calculated using the Euclidean distance. Often this ratio is only modified, when the total curvature of the vessel is calculated in another way, e.g. using the union find table [145], Chain code [4], [147], Hough transform [150] or gradients [36], [20].

REFERENCES

[1] Y. Yin, M. Adel, and S. Bourennane, "Retinal vessel segmentation using a probabilistic tracking method," *Pattern Recognit.*, vol. 45, no. 4, pp. 1235–1244, Apr. 2012.

[2] R. Vega, G. Sanchez-Ante, L. E. Falcon-Morales, H. Sossa, and E. Guevara, "Retinal vessel extraction using lattice neural networks with dendritic processing," *Comput. Biol. Med.*, vol. 58, pp. 20–30, Mar. 2015.

[3] J. Zhang, Y. Cui, W. Jiang, and L. Wang, "Blood vessel segmentation of retinal images based on neural network," *Lecture Notes in Computer Science (Including Subseries Lecture Notes in Artificial Intelligence and Lecture Notes in Bioinformatics)*, vol. 9218. Beijing, China: Image and Graphics, 2015, pp. 11–17.

[4] D. Onkaew, R. Turior, B. Uyyanonvara, N. Akinori, and C. Sinthanayothin, "Automatic retinal vessel tortuosity measurement using curvature of improved chain code," in *Proc. Int. Conf. Electr., Control Comput. Eng. (InECCE)*, Jun. 2011, pp. 183–186.

[5] A. Elbalaoui, M. Fakir, K. Taifi, and A. Merbouha, "Automatic detection of blood vessel in retinal images," in *Proc. 13th Int. Conf. Comput. Graph., Imaging Vis. (CGiV)*, Mar./Apr. 2016, pp. 324–332.

[6] J. Zhao, J. Yang, D. Ai, H. Song, Y. Jiang, Y. Huang, L. Zhang, and Y. Wang, "Automatic retinal vessel segmentation using multi-scale superpixel chain tracking," *Digit. Signal Process.*, vol. 81, pp. 26–42, Oct. 2018.

[7] Y. Zhao, Y. Liu, X. Wu, S. P. Harding, and Y. Zheng, "Retinal vessel segmentation: An efficient graph cut approach with retinex and local phase," *PLoS ONE*, vol. 10, no. 4, Apr. 2015, Art. no. e0122332.

[8] M. Javidi, H.-R. Pourreza, and A. Harati, "Vessel segmentation and microaneurysm detection using discriminative dictionary learning and sparse representation," *Comput. Methods Programs Biomed.*, vol. 139, pp. 93–108, Feb. 2017.

[9] L. Singh, S. R. Sree, P. V. N. S. Likhita, and B. J. Lakshmi, "Robust retinal blood vessel segmentation to detect diabetic retinopathy," *Int. J. Appl. Res. Inf. Technol. Comput.*, vol. 10, no. 3, p. 111, 2019.

[10] R. Turior, D. Onkaew, T. Kondo, and B. Uyyanonvara, "A novel approach for quantification of retinal vessel tortuosity based on principal component analysis," in *Proc. 8th Electr. Engineering/ Electron., Comput., Telecommun. Inf. Technol. (ECTI) Assoc. Thailand-Conf.*, May 2011, pp. 1023–1026.

[11] A. Krestanova, J. Kubicek, J. Timkovic, M. Penhaker, D. Oczka, and J. Vanus, "Modeling and extraction of retinal blood vessels from RetCam 3 based on morphological segmentation," in *Studies in Computational Intelligence*, vol. 830. Berlin, Germany: Springer-Verlag, 2020, pp. 255–263.

[12] A. D. Hoover, V. Kouznetsova, and M. Goldbaum, "Locating blood vessels in retinal images by piecewise threshold probing of a matched filter response," *IEEE Trans. Med. Imag.*, vol. 19, no. 3, pp. 203–210, Mar. 2000.

[13] M. Niemeijer, B. Van Ginneken, and M. J. Cree, "Retinopathy online challenge: Automatic detection of microaneurysms in digital color fundus photographs," *IEEE Trans. Med. Imag.*, vol. 29, no. 1, pp. 185–195, Jan. 2010.

[14] ARIA online. (2006). *Retinal Image Archive*. Accessed: Sep. 18, 2014. [Online]. Available: http://www.eyecharity. Com/aria online.html

[15] E. J. Carmona, M. Rincón, J. García-Feijoó, and J. M. Martínez-de-la-Casa, "Identification of the optic nerve head with genetic algorithms," *Artif. Intell. Med.*, vol. 43, no. 3, pp. 243–259, Jul. 2008.

[16] A. Budai, R. Bock, A. Maier, J. Hornegger, and G. Michelson, "Robust vessel segmentation in fundus images," *Int. J. Biomed. Imag.*, vol. 2013, Dec. 2013, Art. no. 154860.

[17] S. Holm, G. Russell, V. Nourrit, and N. McLoughlin, "DR HAGIS–a fundus image database for the automatic extraction of retinal surface vessels from diabetic patients," *Proc. SPIE*, vol. 4, no. 1, 2017, Art. no. 014503.

[18] F. Oloumi, R. M. Rangayyan, and A. L. Ells, "Assessment of vessel tortuosity in retinal images of preterm infants," in *Proc. 36th Annu. Int. Conf. IEEE Eng. Med. Biol. Soc.*, Aug. 2014, pp. 5410–5413.

[19] T. Chakraborti, D. K. Jha, A. S. Chowdhury, and X. Jiang, "A self-adaptive matched filter for retinal blood vessel detection," *Mach. Vis. Appl.*, vol. 26, no. 1, pp. 55–68, Jan. 2015.

[20] T. Mapayi, J. R. Tapamo, S. Viriri, and A. O. Adio, "Automatic retinal vessel detection and tortuosity measurement," *Image Anal. Stereol.*, vol. 35, no. 2, pp. 117–135, 2016.

[21] H.-C. Han, "Twisted blood vessels: Symptoms, etiology and biomechanical mechanisms," *J. Vascular Res.*, vol. 49, no. 3, pp. 185–197, 2012.

[22] A. E. Kiely, D. K. Wallace, S. F. Freedman, and Z. Zhao, "Computer-assisted measurement of retinal vascular width and tortuosity in retinopathy of prematurity," *Arch. Ophthalmol.*, vol. 128, no. 7, pp. 847–852, 2010.

[23] J. Staal, M. D. Abramoff, M. Niemeijer, M. A. Viergever, and B. van Ginneken, "Ridge-based vessel segmentation in color images of the retina," *IEEE Trans. Med. Imag.*, vol. 23, no. 4,pp. 501–509, 2004.

[24] Y. Zheng, M. H. A. Hijazi, and F. Coenen, "Automated 'disease/no disease' grading of age-related macular degeneration by an image mining approach," *Investigative Ophthalmol. Vis. Sci.*, vol. 53, no. 13, pp. 8310–8318, 2012.

[25] C. G. Owen, A. R. Rudnicka, R. Mullen, S. A. Barman, D. Monekosso, P. H. Whincup, J. Ng, and C. Paterson (2009), "Measuring retinal vessel tortuosity in 10-year-old children: Validation of the computer-assisted image analysis of the retina (CAIAR) program," *Investigative Ophthalmol. Vis. Sci.*, vol. 50, no. 5, pp. 2004–2010, 2009.

[26] H. Kälviäinen, H. Uusitalo, J. Parkkinen. (2009). *Imageret*. [Online]. Available: https://www.it.lut.fi/project/imageret/#DOWNLOAD

[27] T. Kauppi, V. Kalesnykiene, J.-K. Kamarainen. (2008). *DIARETDB0: Evaluation Database and Methodology for Diabetic Retinopathy Algorithms*. [Online]. Available: https://www.it.lut.fi

[28] E. Decencière, X. Zhang, G. Cazuguel, and B. Lay, "Feedback on a publicly distributed image database: The Messidor database," *Image Anal. Stereol.*, vol. 33, no. 3, pp. 231–234, Aug. 2014.

[29] M. O. Hortas and M. Penas Centeno. *VICAVR Database*. Accessed: Jun. 2018. [Online]. Available: http://www.varpa.es/vicavr.html

[30] B. Al-Diri, A. Hunter, D. Steel, M. Habib, T. Hudaib, and S. Berry, "REVIEW–A reference data set for retinal vessel profiles," in *Proc. 30th Annu. Int. Conf. IEEE Eng. Med. Biol. Soc.*, Vancouver, BC, Canada, Aug. 2008, pp. 2262–2265.

[31] J. Zhang, B. Dashtbozorg, E. Bekkers, J. P. W. Pluim, R. Duits, and B. M. ter Haar Romeny, "Robust retinal vessel segmentation via locally adaptive derivative frames in orientation scores," *IEEE Trans. Med. Imag.*, vol. 35, no. 12, pp. 2631–2644, Dec. 2016.

[32] A. Perez-Rovira, T. MacGillivray, E. Trucco, K. S. Chin, K. Zutis, C. Lupascu, D. Tegolo, A. Giachetti, P. J. Wilson, A. Doney, and B. Dhillon, "VAMPIRE: Vessel assessment and measurement platform for images of the REtina," in *Proc. Annu. Int. Conf. IEEE Eng. Med. Biol. Soc.*, Boston, MA, USA, Aug. 2011, pp. 3391–3394.

[33] P. L. Hildebrand, A. L. Ells, and A. D. Ingram, "The impact of telemedicine integration on resource use in the evaluation ROP... analysis of the telemedicine for ROP in Calgary (TROPIC) database," *Investigative Ophthalmol. Vis. Sci.*, vol. 50, p. 3151, Mar. 2009.

[34] E. Grisan, M. Foracchia, and A. Ruggeri, "A novel method for the automatic grading of retinal vessel tortuosity," *IEEE Trans. Med. Imag.*, vol. 27, no. 3, pp. 310–319, Mar. 2008.

[35] A. Christodoulidis, T. Hurtut, H. B. Tahar, and F. Cheriet, "A multi-scale tensor voting approach for small retinal vessel segmentation in high resolution fundus images," *Comput. Med. Imag. Graph.*, vol. 52, pp. 28–43, Sep. 2016.

[36] J. Kubicek, J. Timkovic, M. Penhaker, D. Oczka, V. Kovarova, A. Krestanova, M. Augustynek, and M. Cerny, "Detection and segmentation of retinal lesions in retcam 3 images based on active contours driven by statistical local features," *Adv. Electr. Electron. Eng.*, vol. 17, no. 2. Ostrava, Czech Republic: VSB-Technical Univ. of Ostrava, Jun. 2019.

[37] J. Kubicek, J. Timkovic, M. Penhaker, D. Oczka, A. Krestanova, M. Augustynek, and M. Cerný, "Retinal blood vessels modeling based on fuzzy sobel edge detection and morphological segmentation," *Biodevices*, vol. 1, pp. 121–126, 2019.

[38] J. Kubicek, J. Timkovic, A. Krestanova, M. Augustynek, M. Penhaker, and I. Bryjova, "Morphological segmentation of retinal blood vessels and consequent tortuosity extraction," *J. Telecommun., Electron. Comput. Eng.*, vol. 10, nos. 1–4, pp. 73–77, 2018.

[39] K. S. Sreejini and V. K. Govindan, "Improved multiscale matched filter for retina vessel segmentation using PSO algorithm," *Egyptian Informat. J.*, vol. 16, no. 3, pp. 253–260, Nov. 2015.

[40] R. Turior, P. Chutinantvarodom, and B. N. D. Uyyanonvara, "Automatic tortuosity classification using machine learning approach," in *Applied Mechanics and Materials*. 2013.

[41] M. Vlachos and E. Dermatas, "Multi-scale retinal vessel segmentation using line tracking," *Comput. Med. Imag. Graph.*, vol. 34, no. 3, pp. 213–227, Apr. 2010.

[42] S. Xie and H. Nie, "Retinal vascular image segmentation using genetic algorithm plus FCM clustering," in *Proc. 3rd Int. Conf. Intell. Syst. Design Eng. Appl.*, Jan. 2013, pp. 1225–1228.

[43] S. Pal, S. Chatterjee, D. Dey, and S. Munshi, "Morphological operations with iterative rotation of structuring elements for segmentation of retinal vessel structures," *Multidimensional Syst. Signal Process.*, vol. 30, no. 1, pp. 373–389, Jan. 2019.

[44] E. Imani, M. Javidi, and H.-R. Pourreza, "Improvement of retinal blood vessel detection using morphological component analysis," *Comput. Methods Programs Biomed.*, vol. 118, no. 3, pp. 263–279, Mar. 2015.

[45] G. Chen, M. Chen, J. Li, and E. Zhang, "Retina image vessel segmentation using a hybrid CGLI level set method," *BioMed Res. Int.*, vol. 2017, Aug. 2017, Art. no. 1263056.

[46] Y. Zhao, L. Rada, K. Chen, S. P. Harding, and Y. Zheng, "Automated vessel segmentation using infinite perimeter active contour model with hybrid region information with application to retinal images," *IEEE Trans. Med. Imag.*, vol. 34, no. 9, pp. 1797–1807, Sep. 2015.

[47] H. Gongt, Y. Li, G. Liu, W. Wu, and G. Chen, "A level set method for retina image vessel segmentation based on the local cluster value via bias correction," in *Proc. 8th Int. Congr. Image Signal Process. (CISP)*, Oct. 2015, pp. 413–417.

[48] J. Zhang, Z. Tang, W. Gui, and J. Liu, "Retinal vessel image segmentation based on correlational open active contours model," in *Proc. Chin. Autom. Congr. (CAC)*, Nov. 2015, pp. 993–998.

[49] L. Wang, H. Zhang, K. He, Y. Chang, and X. Yang, "Active contours driven by multi-feature Gaussian distribution fitting energy with application to vessel segmentation," *PLoS ONE*, vol. 10, no. 11, Nov. 2015, Art. no. e0143105.

[50] Z. Xiao, M. Adel, and S. Bourennane, "Bayesian method with spatial constraint for retinal vessel segmentation," *Comput. Math. Methods Med.*, vol. 2013, Jul. 2013, Art. no. 401413.

[51] B. Dizdaro, E. Ataer-Cansizoglu, J. Kalpathy-Cramer, K. Keck, M. F. Chiang, and D. Erdogmus, "Level sets for retinal vasculature segmentation using seeds from ridges and edges from phase maps," in *Proc. IEEE Int. Workshop Mach. Learn. Signal Process.*, Sep. 2012, pp. 1–6.

[52] U. T. V. Nguyen, A. Bhuiyan, L. A. F. Park, and K. Ramamohanarao, "An effective retinal blood vessel segmentation method using multi-scale line detection," *Pattern Recognit.*, vol. 46, no. 3, pp. 703–715, Mar. 2013.

[53] S. Rattathanapad, P. Mittrapiyanuruk, P. Kaewtrakulpong, B. Uyyanonvara, and C. Sinthanayothin, "Vessel extraction in retinal images using multilevel line detection," in *Proc. IEEE-EMBS Int. Conf. Biomed. Health Inform.* Piscataway, NJ, USA: IEEE Press, 2012, pp. 345–349.

[54] M. Ben Abdallah, J. Malek, K. Krissian, and R. Tourki, "An automated vessel segmentation of retinal images using multiscale vesselness," in *Proc. 8th Int. Multi-Conference Syst., Signals Devices*, Mar. 2011, pp. 1–6.

[55] A. Budai, G. Michelson, and J. Hornegger, "Multiscale blood vessel segmentation in retinal fundus images," in *Bildverarbeitung für die Medizin*. Berlin, Germany: Springer, 2010, pp. 261–265.

[56] E. Moghimirad, S. Hamid Rezatofighi, and H. Soltanian-Zadeh, "Retinal vessel segmentation using a multi-scale medialness function," *Comput. Biol. Med.*, vol. 42, no. 1, pp. 50–60, Jan. 2012.

[57] A. S. Jadhav and P. B. Patil, "Preprocessing and segmentation of retina images for blood vessel extraction," in *Communications in Computer and Information Science*, vol. 1036. 2019, pp. 341–348.

[58] U. Ozkava, S. Ozturk, B. Akdemir, and L. Sevfi, "An efficient retinal blood vessel segmentation using morphological operations," in *Proc. 2nd Int. Symp. Multidisciplinary Stud. Innov. Technol. (ISMSIT)*, Oct. 2018, pp. 1–7.

[59] Z. Jiang, J. Yepez, S. An, and S. Ko, "Fast, accurate and robust retinal vessel segmentation system," *Biocybernetics Biomed. Eng.*, vol. 37, no. 3, pp. 412–421, 2017.

[60] M. Frucci, D. Riccio, G. S. D. Baja, and L. Serino, "Using contrast and directional information for retinal vessels segmentation," in *Proc. 10th Int. Conf. Signal-Image Technol. Internet-Based Syst.*, Nov. 2014, pp. 592–597.

[61] A. Kundu and R. K. Chatterjee, "Retinal vessel segmentation using morphological angular scale-space," in *Proc. 3rd Int. Conf. Emerg. Appl. Inf. Technol.*, Nov. 2012, pp. 316–319.

[62] A. Ali, W. M. D. W. Zaki, and A. Hussain, "Retinal blood vessel segmentation from retinal image using B-COSFIRE and adaptive thresholding," *Indonesian J. Elect. Eng. Comput. Sci.*, vol. 13, no. 3, pp. 1199–1207, 2019.

[63] T. Mapayi, S. Viriri, and J.-R. Tapamo, "Adaptive thresholding technique for retinal vessel segmentation based on GLCM-energy information," *Comput. Math. Methods Med.*, vol. 2015, Feb. 2015, Art. no. 597475.

[64] A. Fathi and A. R. Naghsh-Nilchi, "Automatic wavelet-based retinal blood vessels segmentation and vessel diameter estimation," *Biomed. Signal Process. Control*, vol. 8, no. 1, pp. 71–80, Jan. 2013.

[65] J. De, L. Cheng, X. Zhang, F. Lin, H. Li, K. H. Ong, W. Yu, Y. Yu, and S. Ahmed, "A graph-theoretical approach for tracing filamentary structures in neuronal and retinal images," *IEEE Trans. Med. Imag.*, vol. 35, no. 1, pp. 257–272, Jan. 2016.

[66] E. Bekkers, R. Duits, T. Berendschot, and B. ter Haar Romeny, "A multi-orientation analysis approach to retinal vessel tracking," *J. Math. Imag. Vis.*, vol. 49, no. 3, pp. 583–610, Jul. 2014.

[67] D. Chen, L. D. Cohen, and J.-M. Mirebeau, "Vessel extraction using anisotropic minimal paths and path score," in *Proc. IEEE Int. Conf. Image Process. (ICIP)*, Oct. 2014, pp. 1570–1574.

[68] A. Bhuiyan, R. Kawasaki, E. Lamoureux, K. Ramamohanarao, and T. Y. Wong, "Retinal artery–vein caliber grading using color fundus imaging," *Comput. Methods Programs Biomed.*, vol. 111, no. 1. Dordrecht, The Netherlands: Springer, 2013, pp. 104–114.

[69] B. Nayebifar and H. Abrishami Moghaddam, "A novel method for retinal vessel tracking using particle filters," *Comput. Biol. Med.*, vol. 43, no. 5, pp. 541–548, Jun. 2013.

[70] W. Liao, K. Rohr, and S. Wörz, "Globally optimal curvature-regularized fast marching for vessel segmentation," in *Lecture Notes in Computer Science (Including Subseries Lecture Notes in Artificial Intelligence and Lecture Notes in Bioinformatics)* (Lecture Notes in Computer Science), vol. 8149. 2013, pp. 550–557.

[71] Y. Rouchdy and L. D. Cohen, "Geodesic voting for the automatic extraction of tree structures. Methods and applications," *Comput. Vis. Image Understand.*, vol. 117, no. 10, pp. 1453–1467, 2013.

[72] J. Stuhmer, P. Schroder, and D. Cremers, "Tree shape priors with connectivity constraints using convex relaxation on general graphs," in *Proc. IEEE Int. Conf. Comput. Vis.*, Dec. 2013, pp. 2336–2343.

[73] H. Li, J. Zhang, Q. Nie, and L. Cheng, "A retinal vessel tracking method based on Bayesian theory," in *Proc. IEEE 8th Conf. Ind. Electron. Appl. (ICIEA)*, Jun. 2013, pp. 232–235.

[74] V. Kaul, A. Yezzi, and Y. Tsai, "Detecting curves with unknown endpoints and arbitrary topology using minimal paths," *IEEE Trans. Pattern Anal. Mach. Intell.*, vol. 34, no. 10, pp. 1952–1965, Oct. 2012.
[75] N. P. Singh and R. Srivastava, "Retinal blood vessels segmentation by using gumbel probability distribution function based matched filter," *Comput. Methods Programs Biomed.*, vol. 129, pp. 40–50, Jun. 2016.
[76] D. Kumar, A. Pramanik, S. S. Kar, and S. P. Maity, "Retinal blood vessel segmentation using matched filter and Laplacian of Gaussian," in *Proc. Int. Conf. Signal Process. Commun. (SPCOM)*, Jun. 2016, pp. 1–5.
[77] C.-Y. Lu, B.-Z. Jing, P. P. K. Chan, D. Xiang, W. Xie, J. Wang, and D. S. Yeung, "Vessel enhancement of low quality fundus image using mathematical morphology and combination of Gabor and matched filter," in *Proc. Int. Conf. Wavelet Anal. Pattern Recognit. (ICWAPR)*, Jul. 2016, pp. 168–173.
[78] N. P. Singh, R. Kumar, and R. Srivastava, "Local entropy thresholding based fast retinal vessels segmentation by modifying matched filter," in *Proc. Int. Conf. Comput., Commun. Autom.*, May 2015, pp. 1166–1170.
[79] H. Zolfagharnasab and A. R. Naghsh-Nilchi, "Cauchy based matched filter for retinal vessels detection," *J. Med. Signals Sensors*, vol. 4, no. 1, pp. 1–9, 2014.
[80] J. Odstrcilik, R. Kolar, T. Kubena, P. Cernosek, A. Budai, J. Hornegger, J. Gazarek, O. Svoboda, J. Jan, and E. Angelopoulou, "Retinal vessel segmentation by improved matched filtering: Evaluation on a new high-resolution fundus image database," *IET Image Process.*, vol. 7, no. 4, pp. 373–383, Jun. 2013.
[81] J. Kaur and H. P. Sinha, "Automated detection of retinal blood vessels in diabetic retinopathy using Gabor filter," *Int. J. Comput. Sci. Netw. Secur.*, vol. 12, no. 4, pp. 109–116, 2012.
[82] B. Zhang, L. Zhang, L. Zhang, and F. Karray, "Retinal vessel extraction by matched filter with first-order derivative of Gaussian," *Comput. Biol. Med.*, vol. 40, no. 4, pp. 438–445, 2010.
[83] F. M. Villalobos-Castaldi, E. M. Felipe-Riverón, and L. P. Sánchez-Fernández, "A fast, efficient and automated method to extract vessels from fundus images," *J. Vis.*, vol. 13, no. 3, pp. 263–270, Aug. 2010.
[84] A. H. Asad, A. T. Azar, and A. E. Hassanien, "A new heuristic function of ant colony system for retinal vessel segmentation," *Int. J. Rough Sets Data Anal.*, vol. 1, no. 2, pp. 15–30, Jul. 2014.
[85] L. C. Neto, G. L. B. Ramalho, J. F. S. Rocha Neto, R. M. S. Veras, and F. N. S. Medeiros, "An unsupervised coarse-to-fine algorithm for blood vessel segmentation in fundus images," *Expert Syst. Appl.*, vol. 78, pp. 182–192, Jul. 2017.
[86] A. G. Roy and D. Sheet, "DASA: Domain adaptation in stacked autoencoders using systematic dropout," in *Proc. 3rd IAPR Asian Conf. Pattern Recognit. (ACPR)*, Nov. 2015, pp. 735–739.
[87] G. Azzopardi, N. Strisciuglio, M. Vento, and N. Petkov, "Trainable COSFIRE filters for vessel delineation with application to retinal images," *Med. Image Anal.*, vol. 19, no. 1, pp. 46–57, Jan. 2015.
[88] S. Roychowdhury, D. D. Koozekanani, and K. K. Parhi, "Iterative vessel segmentation of fundus images," *IEEE Trans. Biomed. Eng.*, vol. 62, no. 7, pp. 1738–1749, Jul. 2015.
[89] T. Mapayi, J.-R. Tapamo, and S. Viriri, "Retinal vessel segmentation: A comparative study of fuzzy C-Means and sum entropy information on phase congruency," *Int. J. Adv. Robotic Syst.*, vol. 12, no. 9, p. 133, Sep. 2015.
[90] D. Maji, A. Santara, S. Ghosh, D. Sheet, and P. Mitra, "Deep neural network and random forest hybrid architecture for learning to detect retinal vessels in fundus images," in *Proc. 37th Annu. Int. Conf. IEEE Eng. Med. Biol. Soc. (EMBC)*, Aug. 2015, pp. 3029–3032.
[91] S. Sharma and E. V. Wasson, "Retinal blood vessel segmentation using fuzzy logic," *J. Netw. Commun. Emerg. Technol.*, vol. 4, no. 3, pp. 1–11, 2015.
[92] L. Gu and L. Cheng, "Learning to boost filamentary structure segmentation," in *Proc. IEEE Int. Conf. Comput. Vis. (ICCV)*, Dec. 2015, pp. 639–647.
[93] R. Akhavan and K. Faez, "A novel retinal blood vessel segmentation algorithm using fuzzy segmentation," *Int. J. Electr. Comput. Eng. (IJECE)*, vol. 4, no. 4, pp. 561–572, Aug. 2014.
[94] E. Emary, H. M. Zawbaa, A. E. Hassanien, G. Schaefer, and A. T. Azar, "Retinal vessel segmentation based on possibilistic fuzzy c-means clustering optimised with cuckoo search," in *Proc. Int. Joint Conf. Neural Netw. (IJCNN)*, Jul. 2014, pp. 1792–1796.
[95] Y. Wang, G. Ji, P. Lin, and E. Trucco, "Retinal vessel segmentation using multiwavelet kernels and multiscale hierarchical decomposition," *Pattern Recognit.*, vol. 46, no. 8, pp. 2117–2133, Aug. 2013.
[96] Y. Yin, M. Adel, and S. Bourennane, "Automatic segmentation and measurement of vasculature in retinal fundus images using probabilistic formulation," *Comput. Math. Methods Med.*, vol. 2013, pp. 1–16, 2013.
[97] B. S. Y. Lam, Y. Gao, and A. W.-C. Liew, "General retinal vessel segmentation using regularization-based multiconcavity modeling," *IEEE Trans. Med. Imag.*, vol. 29, no. 7, pp. 1369–1381, Jul. 2010.
[98] T. A. Soomro, A. J. Afifi, J. Gao, O. Hellwich, M. Paul, and L. Zheng, "Strided U-Net model: Retinal vessels segmentation using dice loss," in *Proc. Digit. Image Computing: Techn. Appl. (DICTA)*, Dec. 2018, pp. 1–8.
[99] M. Hajabdollahi, R. Esfandiarpoor, K. Najarian, N. Karimi, S. Samavi, and S. M. Reza-Soroushmeh, "Low complexity convolutional neural network for vessel segmentation in portable retinal diagnostic devices," in *Proc. 25th IEEE Int. Conf. Image Process. (ICIP)*, Oct. 2018, pp. 2785–2789.
[100] P. Chudzik, B. Al-Diri, F. Caliva, and A. Hunter, "DISCERN: Generative framework for vessel segmentation using convolutional neural network and visual codebook," in *Proc. 40th Annu. Int. Conf. IEEE Eng. Med. Biol. Soc. (EMBC)*, Jul. 2018, pp. 5934–5937.
[101] S. Guo, K. Wang, H. Kang, Y. Zhang, Y. Gao, and T. Li, "BTS-DSN: Deeply supervised neural network with short connections for retinal vessel segmentation," *Int. J. Med. Informat.*, vol. 126, pp. 105–113, Jun. 2019.
[102] J. I. Orlando, E. Prokofyeva, and M. B. Blaschko, "A discriminatively trained fully connected conditional random field model for blood vessel segmentation in fundus images," *IEEE Trans. Biomed. Eng.*, vol. 64, no. 1, pp. 16–27, Jan. 2017.
[103] A. Dasgupta and S. Singh, "A fully convolutional neural network based structured prediction approach towards the retinal vessel segmentation," in *Proc. IEEE 14th Int. Symp. Biomed. Imag. (ISBI)*, Apr. 2017, pp. 248–251.
[104] J. Zhang, Y. Chen, E. Bekkers, M. Wang, B. Dashtbozorg, and B. M. T. H. Romeny, "Retinal vessel delineation using a brain-inspired wavelet transform and random forest," *Pattern Recognit.*, vol. 69, pp. 107–123, Sep. 2017.
[105] J. Mo and L. Zhang, "Multi-level deep supervised networks for retinal vessel segmentation," *Int. J. Comput. Assist. Radiol. Surg.*, vol. 12, no. 12, pp. 2181–2193, Dec. 2017, doi: 10.1007/s11548-017-1619-0.
[106] A. Lahiri, K. Ayush, P. K. Biswas, and P. Mitra, "Generative adversarial learning for reducing manual annotation in semantic segmentation on large scale miscroscopy images: Automated vessel segmentation in retinal fundus image as test case," in *Proc. IEEE Conf. Comput. Vis. Pattern Recognit. Workshops (CVPRW)*, Jul. 2017, pp. 42–48.
[107] A. Sengur, Y. Guo, U. Budak, and L. J. Vespa, "A retinal vessel detection approach using convolution neural network," in *Proc. Int. Artif. Intell. Data Process. Symp. (IDAP)*, Sep. 2017, pp. 1–4.
[108] J. Song and B. Lee, "Development of automatic retinal vessel segmentation method in fundus images via convolutional neural networks," in *Proc. 39th Annu. Int. Conf. IEEE Eng. Med. Biol. Soc. (EMBC)*, Jul. 2017, pp. 681–684.
[109] Z. Feng, J. Yang, and L. Yao, "Patch-based fully convolutional neural network with skip connections for retinal blood vessel segmentation," in *Proc. IEEE Int. Conf. Image Process. (ICIP)*, Sep. 2017, pp. 1742–1746.
[110] J. H. Tan, U. R. Acharya, S. V. Bhandary, K. C. Chua, and S. Sivaprasad, "Segmentation of optic disc, fovea and retinal vasculature using a single convolutional neural network," *J. Comput. Sci.*, vol. 20, pp. 70–79, May 2017.
[111] T. A. Soomro, A. J. Afifi, J. Gao, O. Hellwich, M. A. U. Khan, M. Paul, and L. Zheng, "Boosting sensitivity of a retinal vessel segmentation algorithm with convolutional neural network," in *Proc. Int. Conf. Digit. Image Computing: Techn. Appl. (DICTA)*, Nov. 2017, pp. 1–8.
[112] D. Francis and J. Jebaseeli, "Fundus image vessel segmentation using PCNN model," in *Proc. Online Int. Conf. Green Eng. Technol. (IC-GET)*, Nov. 2016, pp. 1–5.
[113] N. Memari, A. R. Ramli, M. I. Bin Saripan, S. Mashohor, and M. Moghbel, "Supervised retinal vessel segmentation from color fundus images based on matched filtering and AdaBoost classifier," in *PLoS ONE*, vol. 12, no. 12. Amsterdam, The Netherlands: Elsevier, Dec. 2017, Art. no. e0188939.
[114] H. Fu, Y. Xu, S. Lin, D. W. K. Wong, and J. Liu, "Deepvessel: Retinal vessel segmentation via deep learning and conditional random field," in *Lecture Notes in Computer Science (Including Subseries Lecture Notes in Artificial Intelligence and Lecture Notes in Bioinformatics)* (Lecture Notes in Computer Science), vol. 9901. 2016, pp. 132–139.

[115] Y. Luo, L. Yang, L. Wang, and H. Cheng, "Efficient CNN-CRF network for retinal image segmentation, in *Proc. Int. Conf. Cogn. Syst. Signal Process.*, 2017, pp. 157–165.

[116] P. Liskowski and K. Krawiec, "Segmenting retinal blood vessels with deep neural networks," *IEEE Trans. Med. Imag.*, vol. 35, no. 11, pp. 2369–2380, Nov. 2016.

[117] Q. Li, B. Feng, L. Xie, P. Liang, H. Zhang, and T. Wang, "A cross-modality learning approach for vessel segmentation in retinal images," *IEEE Trans. Med. Imag.*, vol. 35, no. 1, pp. 109–118, Jan. 2016.

[118] H. Fu, Y. Xu, D. W. K. Wong, and J. Liu, "Retinal vessel segmentation via deep learning network and fully-connected conditional random fields," in *Proc. IEEE 13th Int. Symp. Biomed. Imag. (ISBI)*, Apr. 2016, pp. 698–701.

[119] A. Lahiri, A. G. Roy, D. Sheet, and P. K. Biswas, "Deep neural ensemble for retinal vessel segmentation in fundus images towards achieving label-free angiography," in *Proc. 38th Annu. Int. Conf. IEEE Eng. Med. Biol. Soc. (EMBC)*. Piscataway, NJ, USA: IEEE Press, Aug. 2016, pp. 1340–1343.

[120] K.-K. Maninis, J. Pont-Tuset, P. Arbeláez, and L. Van Gool, "Deep retinal image understanding," in *Lecture Notes in Computer Science (Including Subseries Lecture Notes in Artificial Intelligence and Lecture Notes in Bioinformatics)*, (Lecture Notes in Computer Science), vol. 9901. 2016, pp. 140–148.

[121] A. F. Khalaf, I. A. Yassine, and A. S. Fahmy, "Convolutional neural networks for deep feature learning in retinal vessel segmentation," in *Proc. IEEE Int. Conf. Image Process. (ICIP)*, Sep. 2016, pp. 385–388.

[122] A. Wu, Z. Xu, M. Gao, M. Buty, and D. J. Mollura, "Deep vessel tracking: A generalized probabilistic approach via deep learning," in *Proc. IEEE 13th Int. Symp. Biomed. Imag. (ISBI)*, Apr. 2016, pp. 1363–1367.

[123] Z. Yao, Z. Zhang, and L.-Q. Xu, "Convolutional neural network for retinal blood vessel segmentation," in *Proc. 9th Int. Symp. Comput. Intell. Design (ISCID)*, Dec. 2016, pp. 406–409.

[124] D. Maji, A. Santara, P. Mitra, and D. Sheet, *Ensemble of Deep Convolutional Neural Networks for Learning to Detect Retinal Vessels in Fundus Images*. Piscataway, NJ, USA: IEEE Press, 2016.

[125] S. Aslani and H. Sarnel, "A new supervised retinal vessel segmentation method based on robust hybrid features," *Biomed. Signal Process. Control*, vol. 30, pp. 1–12, Sep. 2016.

[126] N. Strisciuglio, G. Azzopardi, M. Vento, and N. Petkov, "Supervised vessel delineation in retinal fundus images with the automatic selection of B-COSFIRE filters," *Mach. Vis. Appl.*, vol. 27, no. 8, pp. 1137–1149, Nov. 2016.

[127] M. Melinscak, P. Prentasic, and S. Loncaric, "Retinal vessel segmentation using deep neural networks," in *Proc. 10th Int. Conf. Comput. Vis. Theory Appl.*, 2015, pp. 577–582.

[128] S. Roychowdhury, D. D. Koozekanani, and K. K. Parhi, "Blood vessel segmentation of fundus images by major vessel extraction and subimage classification," *IEEE J. Biomed. Health Informat.*, vol. 19, no. 3, pp. 1118–1128, May 2015.

[129] S. Wang, Y. Yin, G. Cao, B. Wei, Y. Zheng, and G. Yang, "Hierarchical retinal blood vessel segmentation based on feature and ensemble learning," *Neurocomputing*, vol. 149, pp. 708–717, Feb. 2015.

[130] J. Gu, Z. Wang, J. Kuen, L. Ma, A. Shahroudy, B. Shuai, T. Liu, X. Wang, G. Wang, J. Cai, and T. Chen, "Recent advances in convolutional neural networks," *Pattern Recognit.*, vol. 77, pp. 354–377, May 2018.

[131] C. Zhu, B. Zou, J. Cui, Y. Xiang, and H. Wu, "An ensemble retinal vessel segmentation based on supervised learning in fundus images," *Chin. J. Electron.*, vol. 25, no. 3, pp. 503–511, May 2016.

[132] M. M. Fraz, A. R. Rudnicka, C. G. Owen, and S. A. Barman, "Delineation of blood vessels in pediatric retinal images using decision trees-based ensemble classification," *Int. J. Comput. Assist. Radiol. Surgery*, vol. 9, no. 5, pp. 795–811, Sep. 2014.

[133] Y. Ganin and V. Lempitsky, "N^4-Fields: Neural network nearest neighbor fields for image transforms," *Lecture Notes in Computer Science (Including Subseries Lecture Notes in Artificial Intelligence and Lecture Notes in Bioinformatics)*, vol. 9004. 2014, pp. 536–551.

[134] J. I. Orlando M. Blaschko, "Learning fully-connected CRFs for blood vessel segmentation in retinal images," in *Lecture Notes in Computer Science (Including Subseries Lecture Notes in Artificial Intelligence and Lecture Notes in Bioinformatics)* (Lecture Notes in Computer Science), vol. 8673. 2014, pp. 634–641.

[135] C. Becker, R. Rigamonti, V. Lepetit, and P. Fua, "Supervised feature learning for curvilinear structure segmentation," *Lecture Notes in Computer Science (Including Subseries Lecture Notes in Artificial Intelligence and Lecture Notes in Bioinformatics)* (Lecture Notes in Computer Science), vol. 8149. 2013, pp. 526–533.

[136] A. Chakravarty and J. Sivaswamy, "A novel approach for quantification of retinal vessel tortuosity using quadratic polynomial decomposition," in *Proc. Indian Conf. Med. Informat. Telemedicine (ICMIT)*. Berlin, Germany: Springer-Verlag, Mar. 2013, pp. 7–12.

[137] M. Ceylan and H. B. Yaçar, "Blood vessel extraction from retinal images using complex wavelet transform and complex-valued artificial neural network," in *Proc. 36th Int. Conf. Telecommun. Signal Process. (TSP)*. Berlin, Germany: Springer-Verlag, Jul. 2013, pp. 822–825.

[138] M. M. Fraz, P. Remagnino, A. Hoppe, B. Uyyanonvara, A. R. Rudnicka, C. G. Owen, and S. A. Barman, "An ensemble classification-based approach applied to retinal blood vessel segmentation," *IEEE Trans. Biomed. Eng.*, vol. 59, no. 9. Berlin, Germany: Springer, Sep. 2012, pp. 2538–2548.

[139] B. Zhang, F. Karray, Q. Li, and L. Zhang, "Sparse representation classifier for microaneurysm detection and retinal blood vessel extraction," *Inf. Sci.*, vol. 200, pp. 78–90, Oct. 2012.

[140] D. Marín, A. Aquino, M. E. Gegundez-Arias, and J. M. Bravo, "A new supervised method for blood vessel segmentation in retinal images by using gray-level and moment invariants-based features," *IEEE Trans. Med. Imag.*, vol. 30, no. 1, pp. 146–158, Jan. 2011.

[141] C. A. Lupascu, D. Tegolo, and E. Trucco, "FABC: Retinal vessel segmentation using AdaBoost," *IEEE Trans. Inf. Technol. Biomed.*, vol. 14, no. 5, pp. 1267–1274, Sep. 2010.

[142] A. Yazdanpanah, G. Hamarneh, B. R. Smith, and M. V. Sarunic, "Segmentation of intra-retinal layers from optical coherence tomography images using an active contour approach," *IEEE Trans. Med. Imag.*, vol. 30, no. 2, pp. 484–496, Feb. 2011.

[143] V. V. Makkapati and V. V. C. Ravi, "Computation of tortuosity of two dimensional vessels," in *Proc. 8th Int. Conf. Adv. Pattern Recognit. (ICAPR)*, Jan. 2015, pp. 1–4.

[144] A. Lisowska, R. Annunziata, G. K. Loh, D. Karl, and E. Trucco, "An experimental assessment of five indices of retinal vessel tortuosity with the RET-TORT public dataset," in *Proc. 36th Annu. Int. Conf. IEEE Eng. Med. Biol. Soc.*, Aug. 2014.

[145] N. K. El Abbadi and E. H. Al Saadi, "Automatic retinal vessel tortuosity measurement," *J. Comput. Sci.*, vol. 9, no. 11, pp. 1456–1460, Nov. 2013.

[146] A. Mohsenin, V. Mohsenin, and R. A. Adelman, "Retinal vascular tortuosity in obstructive sleep apnea," *Clin. Ophthalmol.*, vol. 7, pp. 787–792, Nov. 2013.

[147] E. Bribiesca, "A measure of tortuosity based on chain coding," *Pattern Recognit.*, vol. 46, no. 3, pp. 716–724, Mar. 2013.

[148] R. Turior and B. Uyyanonvara, "Curvature-based tortuosity evaluation for infant retinal images," *J. Inf. Eng. Appl.*, vol. 2, no. 8, pp. 1456–1460, 2012.

[149] L. C. Zepeda-Romero, M. E. Martinez-Perez, S. Ruiz-Velasco, M. A. Ramirez-Ortiz, and J. A. Gutierrez-Padilla, "Temporary morphological changes in plus disease induced during contact digital imaging," *Eye*, vol. 25, no. 10, pp. 1337–1340, Oct. 2011.

[150] F. Ghadiri, H. Pourreza, T. Banaee, and M. Delgir, "Retinal vessel tortuosity evaluation via circular Hough transform," in *Proc. 18th Iranian Conf. Biomed. Eng. (ICBME)*, Dec. 2011, pp. 181–184.

[151] J. Tam, K. P. Dhamdhere, P. Tiruveedhula, S. Manzanera, S. Barez, M. A. Bearse, A. J. Adams, and A. Roorda, "Disruption of the retinal parafoveal capillary network in type 2 diabetes before the onset of diabetic retinopathy," *Investigative Ophthalmol. Vis. Sci.*, vol. 52, no. 12, pp. 9257–9266, 2011.

[152] A. Bhuiyan, B. Nath, K. Ramamohanarao, R. Kawasaki, and T. Y. Wong, "Automated analysis of retinal vascular tortuosity on color retinal images," *J. Med. Syst.*, vol. 36, no. 2, pp. 689–697, Apr. 2012.

[153] G. Dougherty, M. J. Johnson, and M. D. Wiers, "Measurement of retinal vascular tortuosity and its application to retinal pathologies," *Med. Biol. Eng. Comput.*, vol. 48, no. 1, pp. 87–95, Jan. 2010.

[154] V. Joshi, J. M. Reinhardt, and M. D. Abramoff, "Automated measurement of retinal blood vessel tortuosity," in *Medical Imaging 2010: Computer-Aided Diagnosis*, vol. 7624, N. Karssemeijer R. M. Summers, Eds. Bellingham, WA, USA: SPIE, 2010, Art. no. 76243A.

[155] A. Salazar-Gonzalez, D. Kaba, Y. Li, and X. Liu, "Segmentation of the blood vessels and optic disk in retinal images," *IEEE J. Biomed. Health Informat.*, vol. 18, no. 6, pp. 1874–1886, Nov. 2014.

[156] D. Kaba, A. G. Salazar-gonzalez, Y. Li, X. Liu, and A. Serag, "Segmentation of retinal blood vessels using Gaussian mixture models and expectation maximisation," in *Health Information Science* (Lecture Notes in Computer Science). Berlin, Germany: Springer, 2013, pp. 105–112.
[157] K. Mittal and V. M. A. Rajam, "Computerized retinal image analysis–A survey," *Multimedia Tools Appl.*, vol. 79 nos. 31–32, pp. 22389–22421, 2020.
[158] D. V. Petrachkov, M. V. Budzinskaya, and K. V. Baryshev, "Current possibilities in visualization of retinal periphery in diabetic retinopathy," *Vestnik Oftalmologii*, vol. 136, no. 4, pp. 272–278, 2020.
[159] D. Mustafi, S. S. Saraf, Q. Shang, and L. C. Olmos de Koo, "New developments in angiography for the diagnosis and management of diabetic retinopathy," *Diabetes Res. Clin. Pract.*, vol. 167, Sep. 2020, Art. no. 08361.
[160] N. Singh, D. Bansal, and D. Nagpal, "Deep learning based retinal vessel segmentation: A review," *Adv. Math., Sci. J.*, vol. 9, no. 6, pp. 3827–3837, 2020.

ALICE KRESTANOVA was born in Opava, Czech Republic, in 1994. She received the bachelor's degree in biomedical technician and the master's degree in biomedical engineering from the VSB - Technical University of Ostrava, Ostrava, Czech Republic, in 2016 and 2018, respectively, where she is currently pursuing the Ph.D. degree in technical cybernetics with a focus on biomedical engineering.

JAN KUBICEK was born in Ostrava, Czech Republic. He received the M.Sc. degree in biomedical engineering, in 2012, and the Ph.D. degree in technical cybernetics specializing in biomedical engineering, in 2018. His research interests include applied image and signal processing in medicine and statistical analysis of biomedical data.

MAREK PENHAKER (Member, IEEE) received the M.Sc. degree in measurement and control, in 1996, and the Ph.D. degree in technical cybernetics from the VSB - Technical University of Ostrava, in 2000. He has been an Associate Professor of biomedical engineering since 2016. He has also been a Professor of biomedical engineering since 2018. His research interests include biomedical engineering, especially medical devices and home telemetry and signal processing.